Summer 7-25-2016

Determining the Power and Energy Capacity of a Battery Energy Storage System Utilizing a Smoothing Feeder Profile to Accommodate High Photovoltaic Penetration on a Distribution Feeder

Osama Mohammed Abbas Aly Mansour
Portland State University

Recommended Citation

Mansour, Osama Mohammed Abbas Aly, "Determining the Power and Energy Capacity of a Battery Energy Storage System Utilizing a Smoothing Feeder Profile to Accommodate High Photovoltaic Penetration on a Distribution Feeder" (2016). *Dissertations and Theses.* Paper 3177.
https://doi.org/10.15760/etd.3174

Determining the Power and Energy Capacity of a Battery Energy Storage System Utilizing a Smoothing Feeder Profile to Accommodate High Photovoltaic Penetration on a Distribution Feeder

by

Osama Mohammed Abbas Aly Mansour

A thesis submitted in partial fulfillment of the
requirements for the degree of

Master of Science
in
Electrical and Computer Engineering

Thesis Committee:
Robert Bass, Chair
Mark Faust
Johnathan Bird

Portland State University
2016

Abstract

Electricity is a perishable commodity; once it is generated it needs to be consumed or stored. Electric energy storage provides both power and energy capacity. Power capacity applications reduce the need for generation, while energy capacity allows for energy consumption to be decoupled from generation. Previous research was done to develop an algorithm for determining the power (MW) and energy (MWh) capacities of a battery energy storage system (BESS) to mitigate the adverse impacts of high levels of photovoltaic (PV) generation. The algorithm used a flat feeder profile, and its performance was demonstrated on the equinoxes and solstices.

Managing feeder power leads to fewer voltage fluctuations along the length of the feeder, potentially mitigating load management issues caused by variability of renewable generation and load profile. These issues include lighting flicker, compressor seizing, equipment shut-off, loss of motor torque ($\tau \propto V^2$), frequent transformer tap changes and even voltage collapse due to loss of reactive power support ($Q \propto V^2$).

The research described in this thesis builds on this algorithm by incorporating a smoothed feeder profile and testing it over an entire year. Incorporating a smoothing function reduces the requisite BESS energy capacity necessary to provide firming and shaping to accommodate the stochastic nature of PV. Specifically, this method is used to conduct a year-long study on a per second basis, as well as a one-minute basis, for a distribution feeder. Statistical

analytical methods were performed to develop recommendations for appropriately sizing the BESS. This method may be used to determine the amount of PV generation that could be installed on a distribution feeder with a minimal investment in the BESS power and energy capacities that would be required to manage the distribution feeder power.

Results are presented for PV penetration levels of 10%-50% of the distribution feeder capacity and show that the use of a smooth feeder profile reduces the required energy capacity by a minimum factor of 10 when compared to a flat feeder profile. Results indicated that it is sufficient to have a one-minute sampling rate, as it provides the necessary granularity to model cloud-induced fluctuations. This method can be applied to any distribution feeder where a load profile and a PV profile are available.

Dedication

To my parents. To my siblings. To my grandparents.

Acknowledgements

I would like to thank Dr. Robert Bass for his guidance, support, and for the various opportunities he's provided me for both personal and educational growth. You have been a great mentor and a truly outstanding role-model. I would also like to thank my thesis committee members: Dr. Robert Bass, Mark Faust, and Dr. Jonathan Bird, for their valuable time and input. Special thanks go to members of the Power Engineering Research group: José Aguilar, Crystal Eppinger, Jordan Landford, Emily Barret, Adam Henke, Timothy Gulzow, Joseph Wilson, and Quinn Sullivan. Much thanks to Nathaniel Krytenberg for shedding a different view on the statistical analysis. I would also like to acknowledge Portland General Electric for the funding provided to the Power Engineering Laboratory to conduct this research. Finally, I would like to thank my family for all the unconditional love and support they continuously provide. Baba, I would not have reached where I am without your guidance. Thank you for being there for me, in times of ease and hardship.

Contents

List of Tables

List of Figures

1 Introduction

The electric power industry has changed dramatically over the past few years, as energy production and energy consumption have experienced a drastic technological shift. Historically, power grids have relied on large thermal power plants, which can be dispatched on-demand, and are able to generate electrical power to fulfill the load demand. Thermal plants typically consume non-renewable resources such as nuclear fuel, natural gas, and coal. However, non-renewable energy resources are not the only means for meeting energy demand; recently an increasing percentage of demand has been met using a combination of intermittent renewable energy sources and peaking power plants. Renewable energy sources include photovoltaic (PV), wind, geothermal, bio-gas, biomass, solar thermal with storage and ocean thermal energy conversion. [1–3] Peaking facilities include hydroelectric power houses, turbine and reciprocating gas power plants, and energy storage units.

Recently, there has been strong interest in solar photovoltaic, likely associated with the exponential decay of capital cost, particularly at the distribution level. The cost of solar generation has decreased by a factor of five in the last fifteen years, and is expected to drop by another factor of three in future. [4] As installed capacity of stochastic, non-dispatchable electrical energy resources increases, the challenges to balancing authorities, dispatchers and marketer's increase. The problems become particularly acute for participants operating within hourly or sub-hourly trading markets. [5, 6]

Solar power generation is intermittent, meaning that the resource varies seasonally, diurnally, and on a sub-hourly timescale. Partial shading of PV modules results in lower energy production, which induces power fluctuations within the system. As the incident solar radiation on a PV generating facility changes, the power generated by the facility can change quite rapidly. The bulk-power system must be designed to provide resource adequacy and have sufficient reserves to accommodate this variability and uncertainty. [7, 8]

System reliability of a transmission network needs to be maintained from facilities and control systems operating within an interconnected electric energy transmission network and electric energy from generation facilities. The availability of generating resources affects a dispatcher's options for maintaining balance between generation and consumption, and a marketer's ability to satisfy contractual energy delivery obligations. Consequently, more spinning reserves, unloaded generation that is synchronized and ready to serve additional demand, must be held in order to ensure reliability as the penetration level of non-dispatchable renewable energy resources grows. [9–13]

A variety of research has been conducted on the feasibility of integration of battery energy storage systems (BESS), as an operating reserve, to mitigate the impacts of high levels of PV penetration. The following sections detail applications of energy storage, and concepts of PV generation.

1.1 Energy Storage Applications & Concepts

Energy storage surrounds us in numerous applications. These applications range from small-scale portable electronics that use batteries, or conversely, large-scale applications that use BESS as a supplemental operating reserve. The future of energy storage is aimed towards: a broadly deployable asset for enhancing renewable penetration, helping reduce coal, oil, and gas consumption. The ability to ensure the resiliency and reliability of the electric grid, and provide smart grid benefits including optimal utilization of demand side assets. [14]

In this section, concepts related to energy storage are discussed. In particular, the following concepts are introduced: PV penetration, power firming, power shaping, power and energy densities of storage, and state of charge (SOC).

1.1.1 Photovoltaic Penetration

Penetration is the ratio of the rated power output of installed PV capacity, known as "nameplate" capacity, compared to the average daily maximum, also known as "peak load", on a distribution feeder. A low penetration of residential PV systems, with each meeting the proposed standard, should have insignificant effects on the utility. For utility applications, high penetration is defined as the point where the ratio of rated power from PV to peak load exceeds 15%. [8] As penetration level increases, at a certain point fluctuations exceed normal load fluctuations that a utility can follow, and detrimental effects of PV generation will arise. These effects include unusual power flows due to voltage rises, sags, and flickers.

Power swings of a larger magnitude may cause loss of service to some loads, which causes a concern of grid stability and power quality that affect protection and coordination.

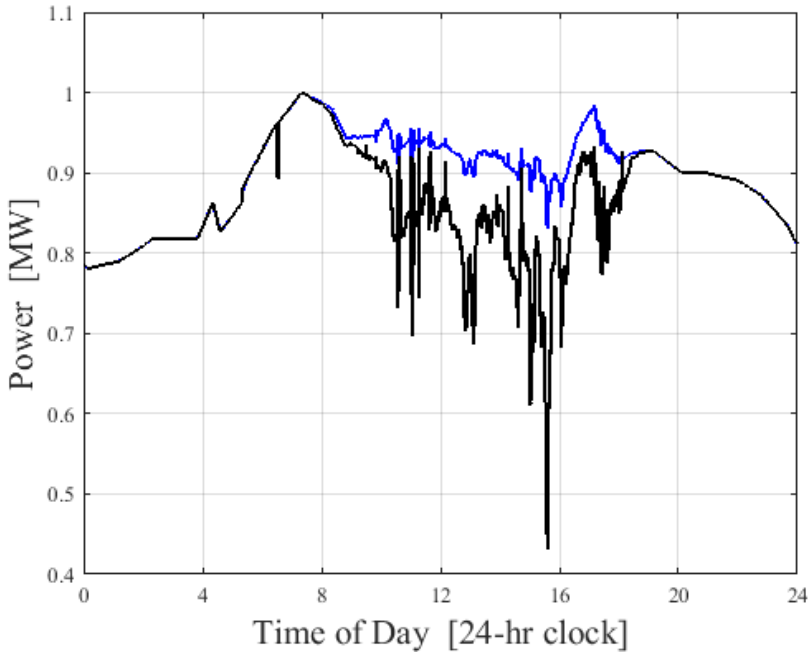

Figure 1.1: PV Penetration Levels - Normalized Scale Comparison of 10% PV Penetration to 50% PV Penetration for a sample day at the Salem Smart Power Plant.

Figure 1.1 shows a comparison of 10% and 50% levels of PV Penetration at the Oxford-Rural distribution feeder in Salem, Oregon. The effects of the cloud-induced fluctuations are amplified. These effects could have significant operational and economic consequences to the utility. [8, 15]

1.1.2 Firming

Capacity firming describes the process of smoothing fluctuations in the intermittent power output of variable generation, in order to mitigate intra-hour fluctuations. Intra-hour fluctuations occur on the order of seconds to minutes. Providing power firming to mitigate

intra-hour fluctuations has a number of positive impacts. Firming reduces fluctuations in customer voltage while concurrently decreasing wear-and-tear on voltage-regulating equipment.

Figure 1.2 shows an ideal days insolation profile with no cloud coverage, and shows the necessary power and energy that would be provided by energy storage to mitigate the stochastic nature of PV generation. Therefore, reducing the need for remote generating facilities. Thereby, opening up transmission corridors and reducing transmission losses. These benefits, taken together, help balancing authorities better accommodate power fluctuations associated with loads and renewable generation, ultimately increasing the potential penetration level of renewables. [16, 17]

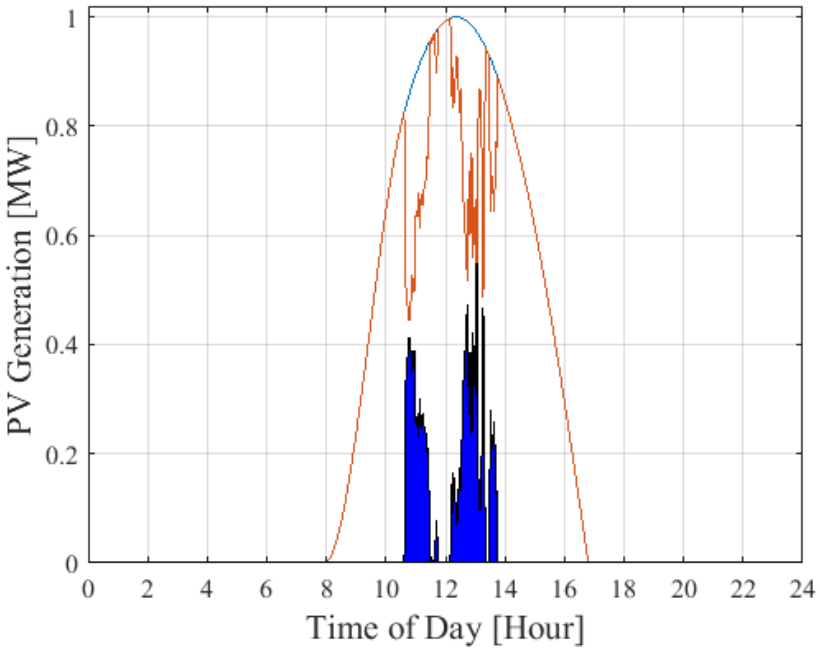

Figure 1.2: Capacity Firming - Ideally, insolation for a day with no clouds shown (in blue) has no fluctuations, a day with cloud-induced coverage shown (in red) causes fluctuations, and shown (in solid blue) is necessary generation provided by energy storage to mitigate the effects of the fluctuations.

1.1.3 Shaping

BESS can be used as their own source of distributed generation (DG). This is done through capacity shaping, which describes the process of shifting power output, in particular, inter-hour fluctuations, which are usually associated with load shifting. Inter-hour fluctuations are slower fluctuations that occur on the order of an hour or longer. Slower fluctuations occur as a result of time of day, day of the week, and weather. [17]

Figure 1.3 demonstrates the ability of a BESS to mitigate inter-hour fluctuations. The regular load profile of the plant is shown on the right. On the left, at the plant bus, the shaved profile is shown vs the original load profile at the plant. The BESS is able to come online as an additional generation resource that is able to provide peak shaving. These peaks are usually associated with times where people are getting off work and consume more power and energy.

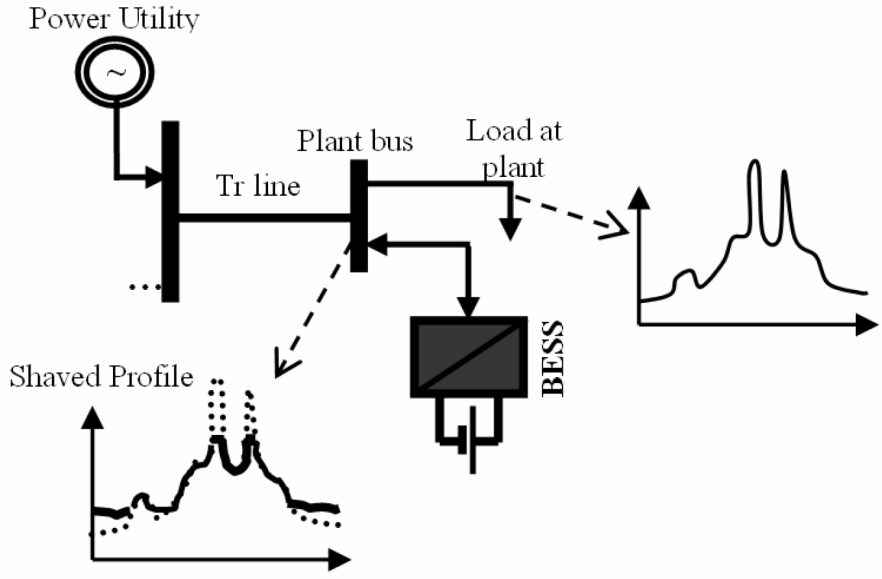

Figure 1.3: Power Shaping - A comparison of a distribution feeder with a BESS to demonstrate the capability of power shaping. To the right is the regular load that would be seen at the distribution feeder, and to the left is the same load with a shaved profile due to power provided by the BESS. [18]

Power shaping allows the power profile to be reduced at peak hours; power firming smooths fluctuations due to intermittent power output.

1.1.4 Power & Energy Densities

Power density is the amount of power that can be delivered from a storage system on a per unit mass or per unit volume basis. Similarly, energy density is the amount of energy that can be stored by a storage system on a per unit mass or per unit volume basis. These are known as gravimetric and volumetric power/energy densities, respectively.

Closely related to energy and power density are footprint and space requirements for energy storage. These criteria are important to consider, particularly in situations where space is valuable or limited, or if weight is an important factor. Depending on the storage technology, space constraints may indeed be a challenge, especially in urban areas. [19] In general, for utility applications, power and energy densities are not significant concerns.

1.1.5 State of Charge

There are a variety of BESS technologies, differentiated by their reaction chemistries. Chemistry type affects the power and energy of a BESS. The BESS chemistry also affects the charge and discharge rates of a BESS, and can change the operational range of a BESS. The BESS cycle life is defined as the number of of complete charge/discharge cycles that the battery is able to perform before its nominal capacity falls below 80% of its initial rated capacity. The factors that affect the cycle life of a battery are time and the number of charge/discharge cycles complete. These can be measured through the state of charge

(SOC), which is the ratio of the BESS charge level expressed as a percentage of the nominal capacity. Another method of quantifying a stored charge is the depth of discharge (DOD), which is calculated as $DOD = 100\% - SOC$. [20]

Once a battery has reached its life cycle, it is usually decommissioned. This is determined by comparing a battery's maximum SOC after it has been manufactured to its SOC after several iterations of charge/discharge cycle. Figure 1.4 shows battery capacity in relationship to cycles of a APR18650 battery cell. The illustration shows the available capacity in coulombs. Once the maximum SOC is less than 80% of the initial SOC the battery is decommissioned. However, it should be noted that in operation 100% DOD is not practical, and therefore the reduction rate may be non-linear. This indicates that the battery may have lived more cycles than the rated life cycle, before the maximum capacity drops to 80%. [21]

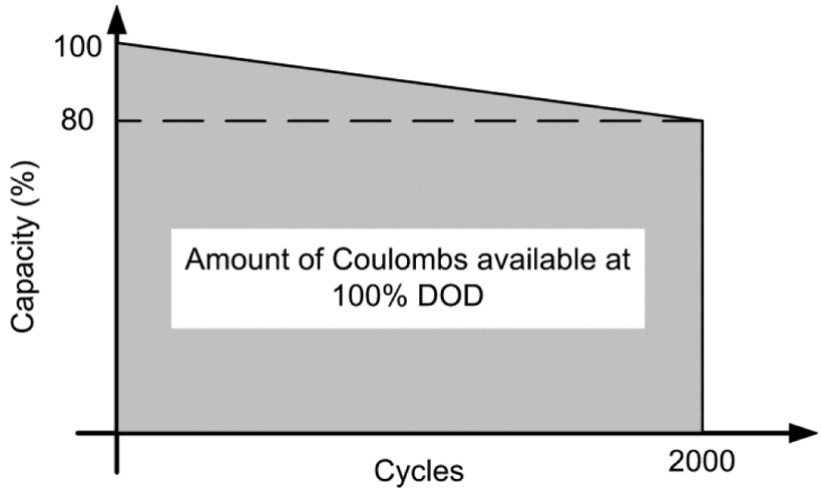

Figure 1.4: Battery Cycle Life of a APR 18650 - The working range of a battery is determined by the SOC, maximum initial charge. This particular battery chemistry typically lasts around 2,000 cycles at 100% DOD. [21]

1.2 Photovoltaic Concepts

In this section, concepts of solar panels are explained, specifically: solar insolation profile, atmospheric effects, and panel placement.

1.2.1 Solar Insolation

Solar irradiance is the amount of power that impinges upon a surface (W/m^2). Solar irradiation is the measure of energy density of sunlight and is measured in (Wh/m^2). Energy is power integrated over time, therefore, irradiation is the integral of irradiance. Irradiance and irradiation relate directly to available sunlight. Therefore, these values change based on the latitude location on the earth, the time of year, and weather conditions. Figure 1.5 shows the solar altitude in comparison to the solar azimuth at 40° latitude for different months of the year. This diagram shows a representation on how the amount of energy impinging upon a surface changes over the year as the earth rotates around the sun and tilts about its axis.

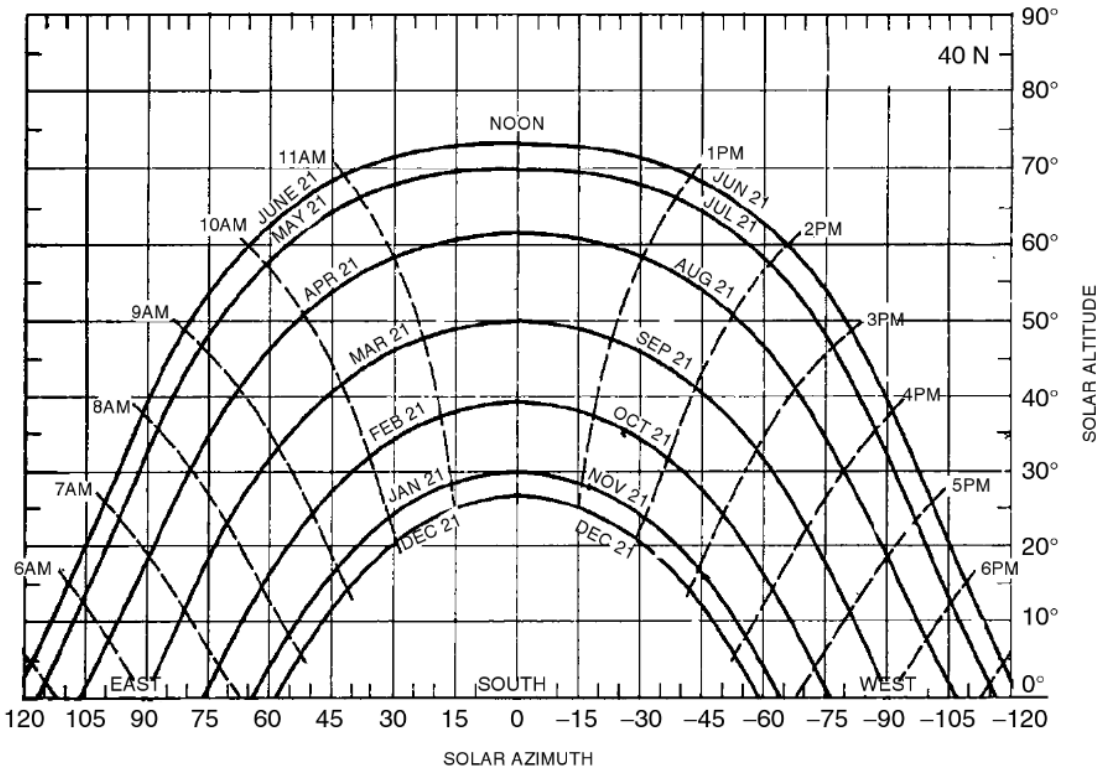

Figure 1.5: Solar Azimuth and Solar Altitude Relationship at $40°$ Latitude - The sun path diagram showing solar altitude and azimuth angles for $40°$ latitude is shown in this figure for representing different times of the day and different months of the year. [22]

1.2.2 Atmospheric Effects on Sunlight

Sunlight that reaches the earth's surface without scattering is referred to as direct or beam radiation. Scattered sunlight is referred to as diffused radiation. Sunlight that is reflected off the ground is albedo radiation. The sum of these three components is called global radiation. These concepts are important because the amount of sunlight that gets scattered or absorbed is dependent on the path through the atmosphere. The intensity of global radiation is $1,367(W/m^2)$ at the top of the atmosphere. Once absorption has been accounted for this value is further reduced to $1,000(W/m^2)$ at sea level. Equation 1.1 gives the relationship

of intensity, *I*. The equation takes into account the reduction at sea level to be reduced to 70% of its value, and takes into account different air masses, $airmass(AM) = 1$; air mass is less than unity at higher altitudes. [23]

$$I = 1367 \times (0.7)^{(AM)^{0.678}} \tag{1.1}$$

1.2.3 Panel Placement

Panels are usually south facing or west facing. The difference in placement can change the insolation by approximately one solar hour, which alters when the maximum power point is seen. In western Oregon, a west facing PV placement is favored if south is unavailable because of the tendency for overcast skies in the morning (east) during summer time. Figure 1.6 shows an example of south-facing vs west-facing panel placement taken from Sacramento, CA. [23]

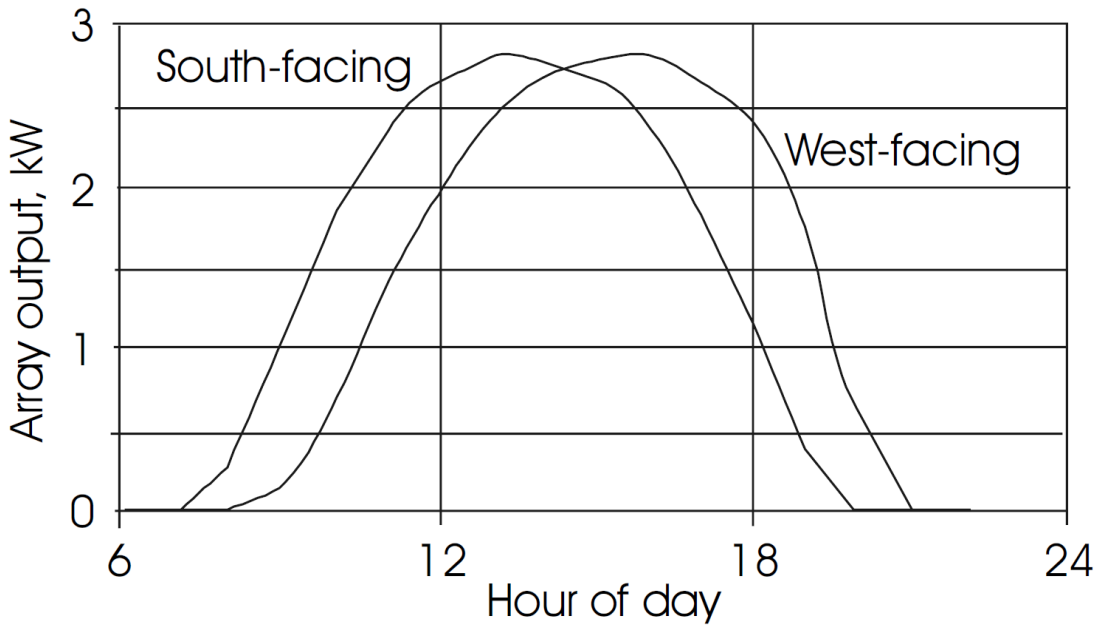

Figure 1.6: South-facing Vs West-facing PV Panels - Comparison of power output and energy output for South- and West-facing PV systems in Sacramento, CA. during the summer. The south-facing system produced 22,417 Wh and the west-facing system produced 22,192 Wh. (Courtesy of Roger [23])

The maximum insolation can be calculated for any direction. [22] First, the latitude, ϕ, of the location needs to be determined. The solar declination, δ, can be calculated through the use of Equation 1.2, where *n* is day of the year.

$$\delta = 23.45^{\circ} sin\left[\frac{360(n-80)}{365}\right] \tag{1.2}$$

The time of day, in local time, for peak PV system output needs to be determined. The local time can be converted to solar time, which is based on previously determined site latitude. The hour angle, w, is the difference between noon and the desired time of day in terms of a 360° rotation in 24 hours, which can be calculated using Equation 1.3. [23]

$$w = \frac{12-T}{24} \times 360^{\circ} = 15\,(12-T)^{\circ} \tag{1.3}$$

Finally, the position of the sun can be tracked in terms of solar altitude, α, and azimuth angle, ψ, through Equations 1.4 and 1.5.

$$\sin\alpha = \sin\delta\sin\phi + \cos\delta\cos\phi\cos w \tag{1.4}$$

$$\cos\psi = \frac{\sin\alpha\sin\phi - \sin\delta}{cos\alpha\cos\phi} \tag{1.5}$$

1.3 Research Objectives

The Portland General Electric (PGE) Salem Smart Power Project (SSPP) features a 5 MW, 1.25 MWh lithium ion battery energy storage system (BESS), located on the Rural distribution feeder at PGE's Oxford substation in Salem, Oregon. Since its commissioning in 2013, the SSPP has helped establish the value of integrating BESS onto distribution feeders. BESS are capable of providing a number of ancillary services, including frequency regulation, economic arbitrage, voltage regulation, and the firming and shaping of power. The objective of the work presented in this thesis is to develop tools to quantify the required power (MW) and energy (MWh) capacities of a BESS to accommodate a particular PV penetration level on a distribution feeder. These tools could then be used by PGE to facilitate greater integration of renewable energy generation systems within their balancing area.

This is done by using a previously-developed SSPP plant model, SSPP load data, and local insolation data to develop a method for determining the BESS MW and MWh capacities

that would be required to provide firming against PV and load fluctuations while also shaping the power profile of a distribution feeder.

1.4 Thesis Statement

The purpose of this thesis is to develop and assess a method to determine power (MW) and energy (MWh) capacities of a battery energy storage system (BESS), given an annual feeder loading profile and annual PV insolation data. An integration algorithm is then used to establish the desired feeder profile (DFP). Statistical methods are used to select the MW and MWh capacities. Variations of the integration algorithm are explored and their effects on the MW and MWh capacities are presented.

2 Battery Energy Storage Background

This section provides a survey of published research on BESS, including that conducted by the Portland State University Electrical and Computer Engineering Department's Power Engineering Laboratory.

2.1 Previous Work by Our Group

In previous work, our group developed a BESS s-domain model and PI (proportional-integral) compensator for the PGE SSPP. [16] The group also developed a method for determining BESS MW and MWh capacities based on a flat DFP. [24] These are discussed in this section.

2.1.1 BESS Model Development

In previous work, our group developed a compensation architecture and firming strategy for the Salem BESS. [16] The compensator takes real-time inputs, specifically load and solar generation, and makes plant output adjustments to firm power fluctuations at the substation. In order to ensure appropriate compensation of the BESS to a time-varying reference input signal, a model of the plant is required. With an accurate representation of the plant, it is then possible to explore various compensator types and tune compensator parameters. [16] The plant and PI models are shown in the closed-loop feedback control

system in Figure 2.1; $R_{BESS}\,(s)$ is the reference signal that is provided to the control system, shown in Equation 2.1. $G_{PI}\,(s)$ is the PI compensator designed to provide a specific gain and phase shift, $G_{BESS}\,(s)$ is the plant model, and $P_{BESS}\,(s)$ is the power output response from the BESS. The DFP calculation is represented in Equation 2.2, where T represents increments of a smooth DFP.

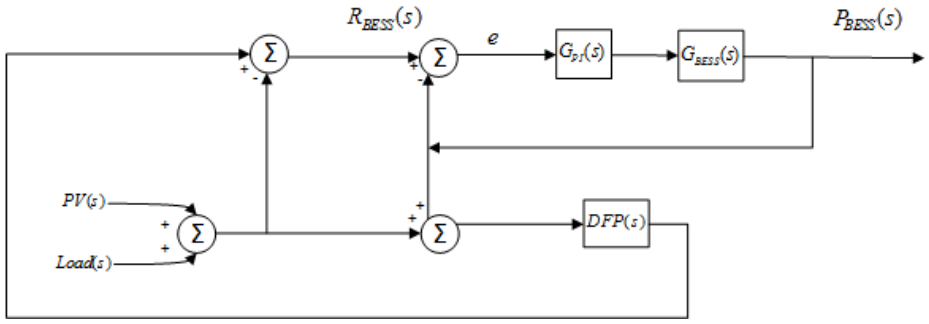

Figure 2.1: Proposed Control Architecture for the BESS - This figure shows the feedback and control loop proposed to control the BESS.

$$R_{BESS} = DFP - (PV + Load) \tag{2.1}$$

$$DFP = \frac{1}{T}\sum (P_{BESS} + PV + Load) \tag{2.2}$$

2.1.1.1 BESS Plant Model

A plant model, G_{BESS}, is developed to determine the characteristics of PGE's SSPP BESS. A second-order transfer function, given in Equation 2.3, is used to model overshoot and oscillations, which a first-order model cannot represent. The undamped natural frequency, ω_n, determines how fast the system oscillates during any transient response. The damping

ratio, ξ, determines how much the system oscillates as the response decays towards toward steady state. [25] To determine these values the SSPP BESS is subject to frequency response tests and step response tests.

$$G_{BESS}(s) = \frac{\omega_n^2}{s^2 + 2\xi\omega_n s + \omega_n^2} \tag{2.3}$$

For the frequency response tests, controlled outputs were measured with respect to the reference input; a second-order transfer function is then derived that best fits phase and magnitude data points. For the step response testing, two tests were conducted, increment and decrement reference steps; overshoot, rise time and settling time were measured. From these measurements two second-order transfer functions were derived, one for increment step test and the other for the decrement step test.

The three second-order transfer functions from the tests conducted were compared, and were found to be very similar, so the average of the three were taken as the representative plant model. For the general second-order transfer function in Equation 2.3, the damping coefficient used is ξ = 0.76 and ω_n = 0.245 as the undamped natural frequency.

The plant model, G_{BESS}, is specific to PGE's SSPP BESS. The derived second-order transfer function is used to determine the MW and MWh capacity for a BESS to compensate PV and load fluctuations. [26]

2.1.1.2 BESS PI Compensator

The PI compensator was tuned to control the plant transient response and eliminate steady-state step response error. The proportional controller compensates the transient charac-

teristics while the integral controller eliminates steady-state step response error. The PI compensator proves sufficient to demonstrate that the BESS can provide firming against PV- and load-induced power fluctuations. [26] The general structure for the PI compensator is given in Equation 2.4.

$$G_{PI}(s) = K_P + \frac{K_I}{s} \tag{2.4}$$

In order to determine the most robust compensator the sensitivity of the compensator to perturbations in the plant model parameters were modeled in MATLAB and Simulink. The proportional and integral compensator gain settings were tuned to $K_P = 0.39$ and $K_I = 0.06$, respectively.

2.1.1.3 Model Performance

The model performance was tested using Simulink and MATLAB. Tests were conducted over sample days. The tests used an existing load profile from the SSPP that was combined with an existing PV profile for the same day. A reference input signal to the BESS was established using 15 minute and 30 minute smoothing profiles. Figure 2.2 shows the response of the PID (proportional–integral–derivative) compensator to the 15 minute smoothing profile. The battery output, shown in blue, is firming the feeder profile following the 15 minute reference input, shown in yellow. It can be seen that the battery is able to firm the power delivered to the feeder through charging and discharging in response to the reference signal. The output of the system for the 15 minute and 30 minute intervals, solid green and solid yellow, respectively, do not have the jagged nature that was previously present in the combined

PV and load data. This indicates that the PID-compensated control system has sufficient transient response to charge and discharge the BESS in response to variations in load and PV generation. [16]

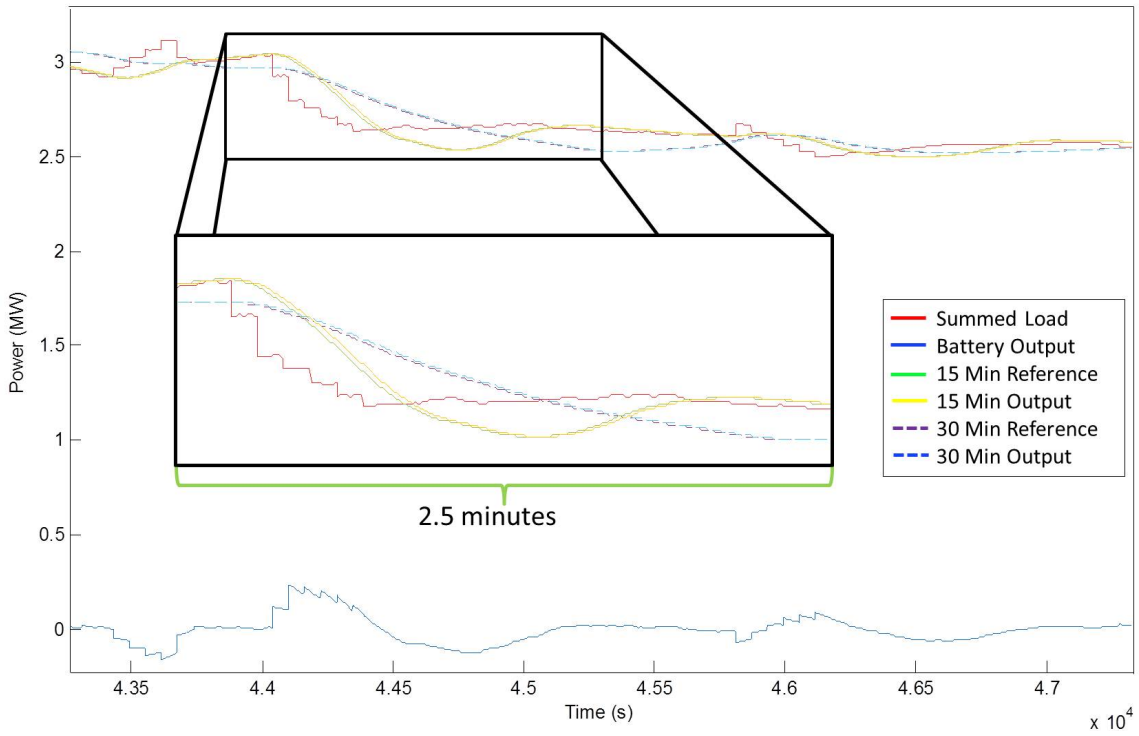

Figure 2.2: PID Compensator Following Testing - PID output following the reference signal: The uncompensated feeder power profile (solid *red*) represents the jagged nature of the *Summed Load*. The control system is guided by a smoothed reference input signal (solid *green* and dashed *purple*). A control system with a well-tuned compensator produces a firmed feeder power output (solid *yellow* and dashed *blue*), that follows the reference input and contrasts sharply with *Summed Load*.The BESS output (solid *blue*) assumes the jagged profile that would otherwise appear in the feeder power profile.

2.1.2 Flat Desired Feeder Profile

In our previous work, our group used a simple, flat desired feeder profile (DFP) as the target feeder power profile. [24] A flat DFP means that the feeder power is constant throughout the day. When loading exceeds the DFP, the BESS discharges, thereby coming online as an additional generation resource to balance the load. When feeder loading falls below the

desired feeder profile, the BESS provides extra loading, drawing power from the feeder as it charges.

The flat DFP was calculated using the average of the net load for a representative day in a season. This straight-line average represents the ideal target value at which the gross energy consumed by the BESS would equal the gross energy produced by the BESS over a day. This straight line DFP is shown in Figure 2.3. The role of the BESS is to charge and discharge in order to balance the stochastic load and generation profiles against the constant DFP.

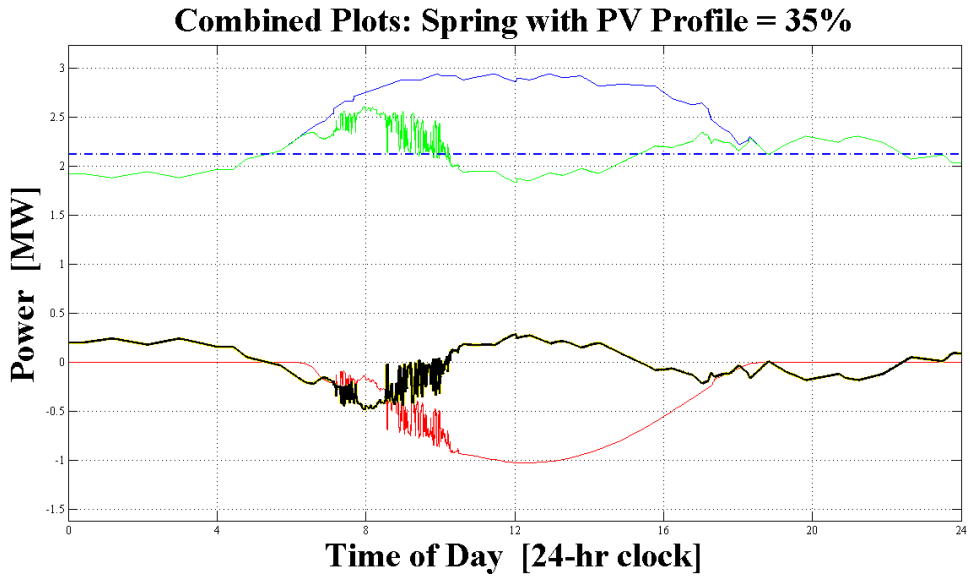

Figure 2.3: Flat DFP - Given a flat DFP, as well as the net loading (PV plus load) for a particular season, a BESS reference signal can be generated. The BESS reference signal then drives the BESS controller to make up the difference between the desired feeder profile and the net load. From these curves, we can determine the optimal PV penetration for a particular feeder and the MW and MWh capacity required of a BESS to achieve that penetration. Key: load (blue), PV (red), net load (green), desired feeder profile (DFP, dash blue), BESS input reference signal (yellow) and BESS response (black).

Figure 2.3 shows the feeder load, PV generation, net load, DFP, and the BESS input reference signal. The flat DFP balances the MWh capacity required to charge the BESS

against that to discharge the BESS. The difference between the DFP and the net load (load minus PV) determines the BESS reference signal, $R_{BESS}\,(s)$, which is fed into the BESS plant model. As seen in Figure 2.3, the controlled signal, $P_{BESS}\,(s)$, closely follows the reference signal, which indicates that the BESS is able to accommodate the PV and load fluctuations.

This BESS reference signal mirrors the curve of the net load. However, as the net load is balanced with respect to the DFP, the BESS reference signal is balanced with respect to a straight line with a zero value. Thus, ideally the periods of charging and discharging should be nearly equivalent.

The flat DFP provides both firming and shaping by smoothing out cloud-induced intra-hour fluctuations and providing inter-hour energy shifting. Which, accommodates the stochastic effects of renewable energy generation. This aforementioned work used a solar insolation envelope profile, which was calculated based on the peaks of the solar data obtained, and did not adequately represent the local insolation profile. As well, the analysis was applied to just four "representative" days of the year, one from each solstice and equinox, to test the MW and MWh sizing strategies. This analysis was insufficient, as a season average does not provide adequate insight into the selection of MW and MWh BESS capacities.

Nor is a flat DFP ideal. For this thesis work, it was hypothesized that a desired feeder profile (DFP) more closely shaped to approximate the net load would be able to facilitate the integration of high levels of PV penetration with less MW and MWh capacities for the BESS. This work focuses on developing DFPs that provide firming, but much less shaping,

by integrating the past 15 to 90 minutes of feeder power demand to provide a projection for future power demand on a minute-by-minute basis. Focusing on firming eliminates short-term fluctuations of customer voltage profiles. Intra-hour voltage fluctuations will still occur, but doing so should result in less required BESS capacity, particularly energy capacity. [26]

2.2 Published Research

This section provides a summary of widely referenced work pertaining to BESS implementations. It also provides a summary of the techniques used to implement the statistical analysis portion of this study.

2.2.1 BESS Implementations

Engineers at PGE subjected the SSPP BESS to battery inverter system (BIS) tests to verify possible integration with the grid and to understand the system's ability to respond to transactive incentive signals (TIS) for charging and discharging. The tests demonstrated that the SSPP BESS had a larger capacity than for what it was rated. This is a result of the manufacturer adding safety margins in order to ensure that the Lithium ion battery chemistry does not degrade under any charge or discharge schema. Lithium ion battery discharge and charge should remain within 20%-80% SOC, to avoid degradation. Tests concluded that the actual available energy is approximately 1800-2000 kWh, not the nameplate rating of 1250 kWh. However, PGE does not have access to this additional energy due to manufacturer control set-points. [27]

Zheng, *et al*, investigate the development of coordinated control tools for next generation PV installations; these consist of PV arrays, BESS (referred to as Energy Storage Units, ESU) and super-capacitors (SC). [28] The objective of their control system is to supply desired active and reactive power to the grid simultaneously to mitigate effects of PV through coordinated control of power electronics. They describe three different coordinated control structures and approaches for grid integration of PV, BESS, and SC. Their description of a typical grid connected PV consists of: solar arrays, BESS, SC, power converters, and an integrated controls system.

The reasoning for adding SCs is that unlike batteries SCs store energy in an electrostatic field. Therefore, they are able to provide faster charge and discharge rates. They claim that the combination of the two is crucial for diverse energy storage needs to meet inter-hour and intra-hour fluctuations. They also classify BESS as having high energy density with "relatively slow response speeds."

An advantage of their design is that they are able to integrate high PV penetrations with the use of their subsystem. However, they do not develop an approach for sizing BESS to integrate a certain level of penetration. The system that they develop contains added costs. SCs are expensive, and the self-discharge rate of SCs are much higher than BESS.

Jayasekara, *et al.*, develop a real power management optimization method that improves voltage profiles of a test feeder with finely distributed PV to minimize losses. [29] They claim that their technique may not be practical for widespread installations of distributed generation, as size and location of the DG units is dependent on customer choice. Their

storage technique utilizes old car batteries that have over 80% SOC remaining. The batteries are integrated with uniformly distributed PV. They determine the number of batteries and locations to be installed using a random number generator to mimic the uncontrolled nature of customer choice. They use a Fourier series approach to represent the battery SOC profile 24 hours ahead of time. They predict the instantaneous battery power needed, SOC, and the peak load demand. Their results, based on day-ahead battery SOC, are sufficient to demonstrate benefits of storage in peak shaving and on the voltage profile of the test feeder when accommodating distributed PV systems.

Jewell, *et al.* investigates the effects of moving clouds on electric utilities with dispersed PV generation. [8] The paper presents the results of simulations to determine the effects of cloud-induced fluctuations. The approach utilizes different penetration levels of aggregate PV over different areas covered by a utility. Simulations vary over different percentages of the sky being covered, different cloud speeds, and the optical transmission properties of different cloud types.

The study concluded that the percentage of possible change drops as the area increases if the geographical density of the PV systems is dispersed. For larger areas, maximum changes in PV output occur within 1-2 minutes. Other important factors noted were: that squall lines, a group of thunderstorm clouds, cause 100% loss in PV generation. They noted that these are not as important as cumulus clouds due to the ease in prediction of such cloud formations. The most important note made is that the maximum PV changes occur during peak insolation times. It was noted the operating penetration varies due to diurnal effects of

PV generation and load profiles. PV penetration becomes significant at the point where the utility has to change its operating practices to accommodate for effects of PV. The swings may cause operation problems, which will more than likely increase operation costs.

Oudalov, *et al.*, presents a sizing methodology and an optimal operation strategy for a BESS to provide peak shaving capabilities. [18] The research conducted is aimed at an industrial level customer to provide a reduction in energy for the customer. The recommended optimal size of the BESS was 0.25 MW for power capacity and 0.75 MWh capacity for energy capacity, and assumed batteries had a life cycle of 20 years. The proposed method was tested with a real industrial customer load profile. However, the proposed solution only offered an annual electricity bill reduction by 8% of the power demand in comparison to a situation without a BESS.

Gurganus presents in his thesis the feasibility of using BESS to decrease the ramp rates of PV power plants on a utility scale level. [30] Simulation techniques of grid-connected PV arrays and a BESS were developed that can be parametrized to different PV setups and different battery chemistries. The main objective of the thesis is to determine the most feasible parameters for a utility by finding: chemistry of BESS, energy capacity of the BESS, energy to be initially stored by the BESS before outputting to the grid, and how much variability the system should attempt to mitigate. One limitation that was mentioned is that the model is not intended to address issues such as reactive power and frequency response. The contribution of the thesis is not intended on providing a cost-benefit analysis of a BESS. The main aim of the research is to find configurations of a potential BESS that would result

in a desirable system output when a BESS is coupled with a utility scale PV plant.

The metrics used in the research for a reasonable configuration of BESS parameters are absolute leveling, reactive leveling, and time-shifting. The absolute leveling application is a scenario similar to that of a flat DFP, where the utility would want a constant output over a certain period of time. The resultant output to the grid would be less during mid-day than the raw PV output, but would be greater in the morning and later in the afternoon. Reactive leveling requires that the worst variations in output be mitigated; this method requires less energy to be stored. Finally, time-shifting represents the times when there is a large difference between peak and off-peak power costs to incentivize storing off-peak power to discharge during peak times.

Results indicated that existing grid connected PV systems are likely to be brought to profitability by installing a BESS. Choice of battery chemistries that resulted in the highest additional revenue were: Sodium Sulfur, Vanadium redox flow batteries, and lead-acid cells. Battery choice is affected by variability in energy capacity measured at approximately 50% of the hourly peak power output of the PV array, and a power output leveling target of approximately the same size. Gurganus concluded that the savings in costs associated with infrastructure and maintenance will begin to grow as we begin to harness energy closer to where we use it.

Nagarajan presents in his thesis the development of a model for the analysis of distributions feeders with high penetration levels of PV generation. [31] The objective of the thesis provides a generalized deployment of Li-Ion BESS to increase the benefits of PV

on a distribution feeder. An approach for sizing and scheduling of the BESS alongside micro-turbines is proposed for reliable operation.

Nagarajan demonstrated the possibility of performing long-term transient analysis using phasors and differential algebraic equations. The work proposed, and validated, the use of active power filters for mitigating the effects of unbalanced PV generators. The work also proposed and implemented optimization methods for sizing and scheduling BESS and micro-turbines using Benders' decomposition. A lithium-ion based energy storage system of 0.5 MW for power, and 1.5 MWh for energy was used for the study. Two scenarios were run: energy shifting and a solar smoothing scenario. Energy shifting scenario was expected to guarantee minimal variation in the charge/discharge rate for the BESS, thus leading to a longer life-time. A solar smoothing scenario was designed to allow the BESS to monitor solar PV output and react immediately to mitigate effects of PV generation. However, both studies were conducted for a single day, December 6th 2012, for the geographic location of Flagstaff, AZ. The BESS accommodated the PV variability in solar smoothing, whereas during the energy shifting scenario the grid fulfilled the PV variability. BESS charged from the PV source and started discharging during the rapid changes in the PV output caused by the cloud-induced fluctuations; grid power drawn to mitigate the load was minimized.

Final results specific to the distribution feeder indicated that the kWh rating of the energy storage system was large for a typical winter month, compared to the rating for a summer month. For the energy shifting scenario, capacities of 0.2 MW and 2.3 MWh were proposed. For the smoothing scenario, capacities of 0.2 MW and 1.7 MWh were proposed. The BESS

were used in conjunction with micro-turbines. However, Nagarajan acknowledges that these values are specific to one day analysis, and concludes that the micro-turbines should be employed to mitigate the variability of PV generation.

Omran, *et al.*, investigate methods to mitigate power fluctuation generated from large grid-connected PV systems. [32] Their methods focus on the use of BESS, the use of dump loads, and the curtailment of generated power by operating the PV system below the maximum power point. The economical aspects are explored, and revenues gained are estimated using a linear programming optimization. Their results concluded that there would be a loss of revenue when fluctuating power from PV is not smoothed. There was a use of different limits of power fluctuation leniency, and it was found that the loss in revenue is higher as the limit is decreased. This was attributed to increases in both power and energy ratings of the BESS. Dumping excess power to satisfy power fluctuation limits and curtailment of the maximum power point resulted in lower revenue losses than with the use of BESS to mitigate the fluctuations. The final recommendation, as to what was most economically viable, is the use of a BESS with power curtailment.

Hirst, *et al.*, define intra-hour and inter-hour load swings. [17] As electricity consumption varies, the grid starts exhibiting load swings on the order of seconds, fast fluctuations, or slower fluctuations that can occur on the order of an hour or longer. Total load is split up in three categories: base load, load change from hour to hour, and finally random fluctuations in load. The focus of the paper is on the latter two.

They define intra-hour load changes as short-term fluctuations, and inter-hour fluctua-

tions are those that occur on a larger time scale. Inter-hour load swings (in MW) have a much greater magnitude than intra-hour changes; the difference is a factor of 15 to 40. The rate of change (MW/min) is much greater for intra-hour changes than for inter-hour changes, with a factor of 3 to 5. The frequency change (sign of the ramp rate), is much greater for intra-hour changes than for inter-hour changes, with a factor of 100.

Yeng, *et al.*, propose a sizing strategy for distributed BESS with high penetration of PV for voltage regulation and peak load shaving. [21] They define problems that high penetration of PV cause, and offer a solution of integrating BESS into PV systems in order to achieve a flexible real power control. The purpose of their research is that the *optimized BESS* has not been considered, and therefore most research usually leads to over-sized BESS, which results in extra cost. They develop a method where the BESS usage, lifetime, and system performance in terms of battery size are analyzed on a set of distribution feeders with existing PV.

The approach uses real annual load profile, PV power profile, and temperature profile; the method is applied on a modified General Electric model. A physical model of a LiFPO4 (lithium-ion phosphate) battery with aging effects was also developed. The cost-benefit analysis is based on a three-step cycle. The profiles are fed into the distribution power system model, which are then compared by the energy management system to bus voltages, SOC. The cost of each battery is calculated under every possible battery size with different PV penetration levels. The cost-benefit BESS size is then derived.

The study focuses on simulations to a single feeder. The feeder length is 6 miles and

the total peak load is 11 MVA. The loads are split up into seven feeders, which, represent a mixture of residential and commercial peak loads, that ran from 0.3 MW to 5MW, with a power factor of 0.92. The seven buses had BESS and hybrid PV connected to them. Four case studies are performed: *Case A*: System performance with and without a BESS, *Case B* BESS lifetime and usage, *Case C* highlight use of on-load-tap-changer and step voltage regulators stress tests with BESS, and finally, *Case D* is a BESS cost analysis. The proposed method is able to obtain BESS cost and benefits of each bus under different PV penetration levels for any selected BESS size. This makes the trade-off between economic profits and operational benefits quantifiable.

Teng, *et al.*, design an optimal charging/discharging scheduling for BESS. [33] This is done such that line loss of distribution systems interconnected with high levels of PV generation can be minimized. They propose mitigation of the intermittent nature of PV generation. This is achieved by charge/discharge scheduling that would be arranged within the hourly market with respect to load variations and intermittent outputs of PV. The proposed mathematical model uses the SOC variation to determine the charging state by determining constant current or constant voltage. Optimal scheduling is then calculated based on solar irradiance. The system was successfully implemented, using C++, and tested with a distribution feeder from Taiwan Power Company. Test results showed that the proposed method has potential in analysis of other BESS applications such as regulation services, voltage support, peak-load shifting, and reliability improvement.

Obi, *et al.*, propose a methodology for calculating the levelized cost of electricity (LCOE).

Specifically, the algorithm is geared towards utility-scale energy storage systems. [12] They found that existing LCOE algorithms are not suitable for storage technologies and do not provide the proper range of inputs needed to assess LCOE for energy storage. LCOE is a means for standardizing metrics when comparing costs of energy systems. The study focused on clarifying cost parity for utility-scale energy storage against the traditional gas peaking facilities. Pumped hydro energy storage, compressed air energy storage, and lead-acid energy storage systems have the most competitive LCOE when base-lined against simple-cycle combustion turbines (SCCT).

SCCT was chosen as a baseline because they determined it as the technology with which utility-scale storage systems must compete. SCCT are used to provide ramping and frequency regulation services for mitigating the stochastic nature of wind and PV generation. Several model variations were conducted, which provided insight on technology-specific impacts on LCOE, such as power and energy capacities.

A sensitivity analysis was conducted demonstrating that the LCOE values have strong sensitivity to three parameters, in particular: storage efficiency, purchasing, and selling price of electricity. Other values that were moderately sensitive were power and energy capital costs, and the capacity factor of a plant. It was recommended that analysts comparing cases take note of these six parameters due to their strong influences on the LCOE algorithm.

It was concluded that battery systems designed to provide bulk energy storage require more energy capacity than systems designed to provide frequency regulation support, or have a higher life cycle than the battery systems and need less replacement. In comparison

to the SCCT baseline set, it was concluded that few battery technologies are currently price competitive.

2.2.2 Data Stratification

The load data used in this thesis work has a bi-modal distribution for the capacity requirements. We hypothesize that this bi-modality results from differences in load between weekdays and weekends. This difference in load consumption may be occurring due to industrial processes being halted during the weekends; almost 26% of energy consumption in Oregon is due to industrial processes. [34] This difference in load would be sufficient enough to cause dual processes resulting in a bi-modal distribution. This is further discussed in Section 5.1

Reichard classifies stratification techniques into two groups: a hybrid type technique used with heterogeneous data; data that belong to different clusters should be as different as possible. The second approach is utilized: the approach is to divide the population into strata or levels, each of which is more or less homogeneous, and then take samples from each stratum. A random sample is drawn from each stratum and then combined with proper weighting into an estimate for the population. With more accurate estimates for each stratum, the estimate of the entire population should be more accurate for a given sample size. [35]

A potential drawback with stratification is that one or more of the sub-samples may be small in size, leading to problems with the reliability of the estimates. Also, the results for each sub-sample are generalizable to only a part of the sample population.

To develop a practical stratified sampling scheme, Särndal, Swensson, and Wretman note that the following three questions must be answered: [36]

1. What variables are to be used for stratification?

2. How should the strata be demarcated?

3. How many strata should there be?

It is important to note that the selection of stratification variables is subjective and based in part on prior knowledge, and subject matter expertise. [36, 37] These questions will be further addressed in Section 4, where discussion of techniques for statistical analysis of the BESS performance and results take place.

2.3 Summary of this section

This section provided a summary of the work done by our group to develop a control architecture for the BESS, the work done to show the model performance of the BESS, and the testing of the proposed model using a flat feeder profile to provide seasonal insight. Work done by other researchers were also presented, which included: tests conducted on BESS to determine SOC, various methods to mitigate the effects of inter-hour fluctuations of PV generation using energy storage, sizing and optimization strategies of a BESS, and LCOE algorithms specific to energy storage. Finally, a summary of data stratification techniques that will be utilized in the analysis portion of the data is also presented.

3 Research Methodology

This section pertains to the method for determining the power and energy storage requirements for a BESS. This is done by acquiring load and PV profiles for 365 days. The PV and load profiles obtained had a sampling rate of one-minute. The method proposed was conducted for a one-second sampling rate and a one-minute sampling rate. Two sampling rates are used to determine if a lower PV sampling rate is necessary to represent cloud-induced PV fluctuations. A 365 day analysis is conducted utilizing a smoothed feeder profile to establish a reference signal to the BESS. The BESS energy and power capacities are then calculated with variance in PV penetration level, 10% to 50% in increments of 5%, based on the feeder size, and variations of the smoothing algorithm. Figure 3.1 shows the process flow diagram of the methodology.

Figure 3.1: Methodology Flow Chart - This flow chart shows the procedure conducted for an annual analysis to recommend MW and MWh capacities to accommodate different PV generation penetration levels on a distribution feeder.

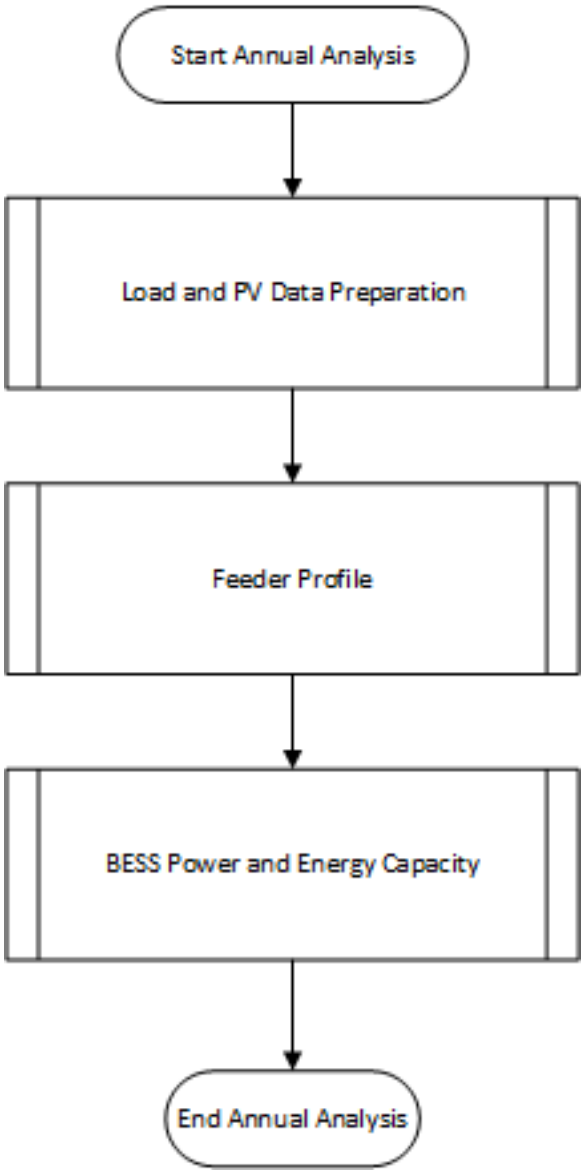

The following sections will be split up in the following manner: load and PV data preparation, the smoothed desired feeder profile, and the calculation of the power and energy requirements.

3.1 Load & PV Data Preparation

The required MW and MWh capacities for a BESS are directly related to the load profile of the system and the PV generation profile. The load profile and PV generation profile are comprised of data covering an entire year. Figure 3.2 details the method used for data preparation of the these profiles.

Figure 3.2: Data Preparation Flow Chart - This flow chart shows the procedure to prepare the PV profile and the load profile to obtain a combined PV and load profile at different PV penetration levels.

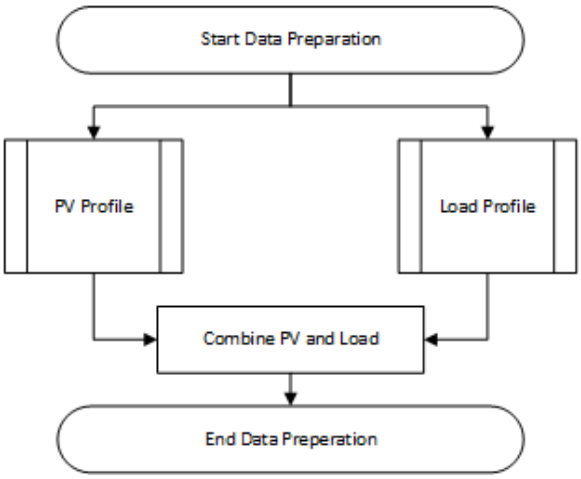

The following sections give specifics for data preparation for a one-second sampling rate and a one-minute sampling rate.

3.1.1 One-Second Sampling Rate

If the PV data sample rate is too low the data cannot represent cloud-induced changes in energy generation. Therefore, high sample-rate data are needed in order to better determine the MW and MWh capacities to compensate rapid load and PV fluctuations. [26] For analysis

purposes, the time span and sample rate of these data sets must align. To deal with the discrepancies in the sampling rate between load and PV generation profiles, a time scale of 86,400 seconds per day was used to represent the load and solar irradiance data. This rate is sufficiently fast to model cloud-induced PV power fluctuations.

Modeling these data sets involved data expansion, interpolation, normalization, and scaling. Once the data were processed, the MW and MWh requirements are determined for 365 days. The following sections discuss the conditioning and processing of the load data, PV data, and the combination these data sets.

3.1.1.1 Load Data

Figure 3.3 shows the procedure conducted to the load profile to obtain a one-second granularity load profile.

Figure 3.3: Load Data Preparation Flow Chart - This flow chart shows the procedure conducted to obtain a load profile with one-second granularity.

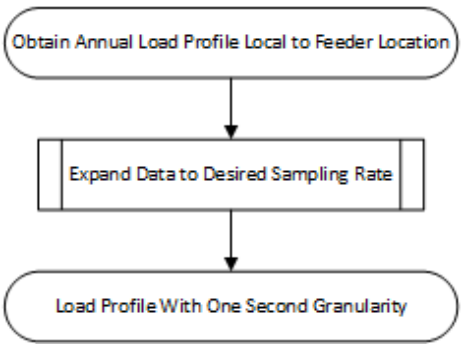

Load data were obtained from PGE's Oxford-Rural feeder for the year of 2012. Oxford is the closest substation to the SSPP BESS, which is on the Rural feeder. The load data are

given in one minute increments from January to December of 2012. The data constitute 1440 data points per day for 366 days; since 2012 was a leap year the last day was omitted to make the data set 365 days. This data set is relevant in order to establish a base line for the feeder to which the SSPP BESS is connected. This gives us an idea of the daily average maximum load that occurs, which can then be used to simulate the effects of variations of PV penetration on the feeder.

The data were prepared for a full year to a time scale of 86,400 seconds a day. This was done by expanding the 1440 points that represented a minute; an assumption was made that the value given from a data set was the constant value over a 60 second scale. ($1440 \times 60 = 86,400 pts$). This process was done for 365 days to create a load profile that has 86,400 seconds per day. The data set was then normalized to be used with other data sets.

3.1.1.2 PV Data

Figure 3.4 shows the procedure conducted to the PV profile to obtain one-second granularity data of the Salem PV profile.

Figure 3.4: PV Data Preparation Flow Chart - This flow chart shows the procedure conducted to obtain a PV generation profile with one-second granularity.

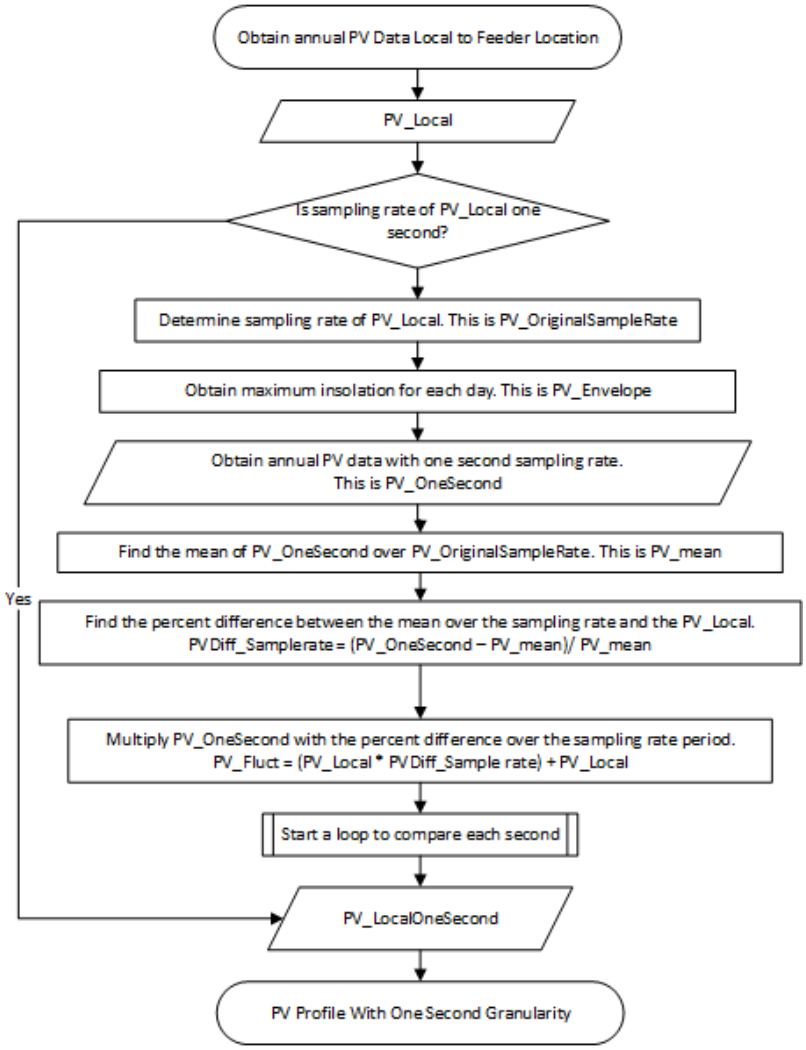

Data were obtained from the University of Oregon Solar Radiation Monitoring Laboratory station located near the SSPP. The Salem PV profile has a sampling rate of one-minute and a range from January to December of 2014; this constitutes 1440 data points per day, for 365 days. [38]

Data were also obtained from an irradiance monitoring station in Oahu, Hawai'i. Oahu

PV data provide a one-second sampling rate, and corresponds to data from 5AM to 8PM. The data set used was from April 2010 to March 2011. [39] Since the sampling rate of the Salem PV data is not fast enough to represent rapid fluctuations such as cloud events, the Oahu PV data were used in combination with the Salem data to provide this level of detail. The Salem data provides the general daily generation shape and the Oahu data provide the rapid fluctuations.

For the Salem PV data processing, the following steps were taken. The first step was extracting data from 5AM to 8PM for 365 days. This is done to match the Oahu provided data. The extracted data are then normalized. A PV envelope was generated, then normalized using location details of SSPP. This was done using the National Renewable Energy Laboratory (NREL) Solar Position (SOLPOS) calculator for the 365 days for the year of 2012. [40] The calculator computes the solar position and intensity from time and place, based on the user inputs. This provides insight that is important for determining the gross behavior of solar irradiance over a year. Figure 3.5 shows a sample day of the generated envelope with the PV profile for that day. For this analysis generation is represented as negative and load consumption as positive.

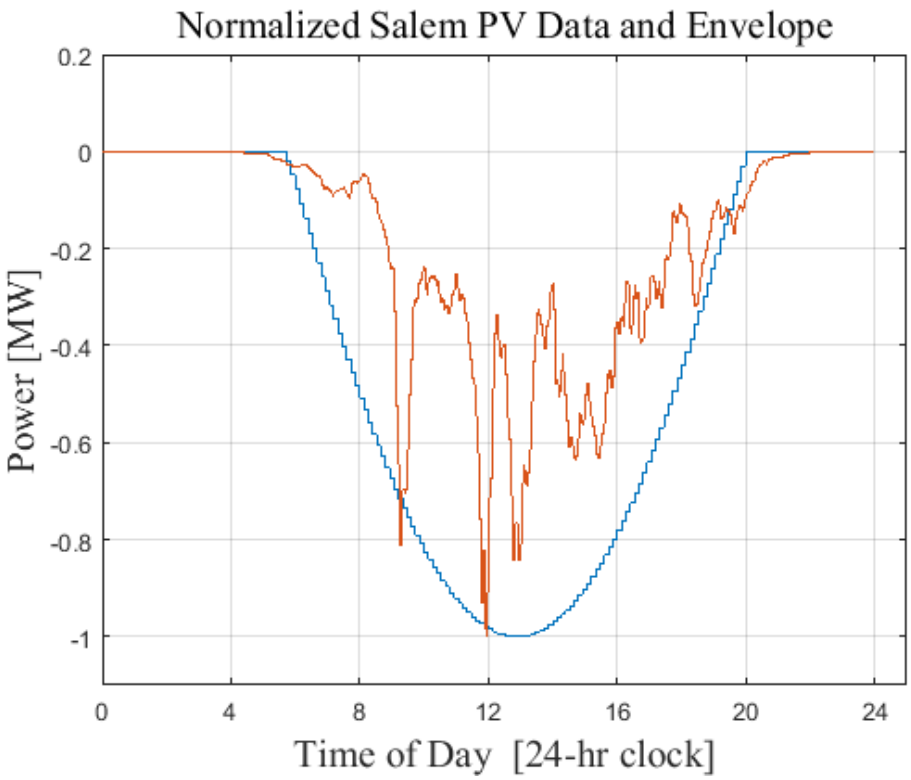

Figure 3.5: This figure shows the PV envelope that was generated by SOLPOS [40], in blue, and the PV data collected from the SSPP [39] with one-minute granularity, shown in red.

The fluctuations of Oahu were calculated by finding the average over the sampling rate period. The change that occurs is then calculated over the period of the sampling rate. The following MATLAB code shows how this is done:

```
y=1; %day
while y < 365+1
    x=1:60; % seconds
    t=1;
              while t <901
                OahuMean_60(x,y)=mean(Oahu(x,y));
                % Find the average of the data over the
                % sampling rate of original data
                 x=x+60;
                 t=t+1;
             end
y=y+1;
end

% Find the rate of change between Oahu Data set,
% and the average over the sampling rate
OahuDiff_60= -(Oahu - OahuMean_60) ./ OahuMean_60;

% Multiply the Salem PV data by the % error from
% SalemPV, and then add back to original Salem PV.
% This is how the fluctuations are imposed.
    SalemFluct= (SalemNormalized .* -OahuDiff_60) + SalemNormalized;
```

Figure 3.6 shows the procedure conducted to $SalemFluct$ to accommodate for the Oahu, HI and Salem, OR differences in solar insolation profiles.

Figure 3.6: PV Data Preparation Flow Chart Showing Accommodation of Oahu and Salem Differences- This flow chart shows the procedure conducted to ensure that the Salem PV data was preserved when the Oahu data was imposed to obtain one-second granularity.

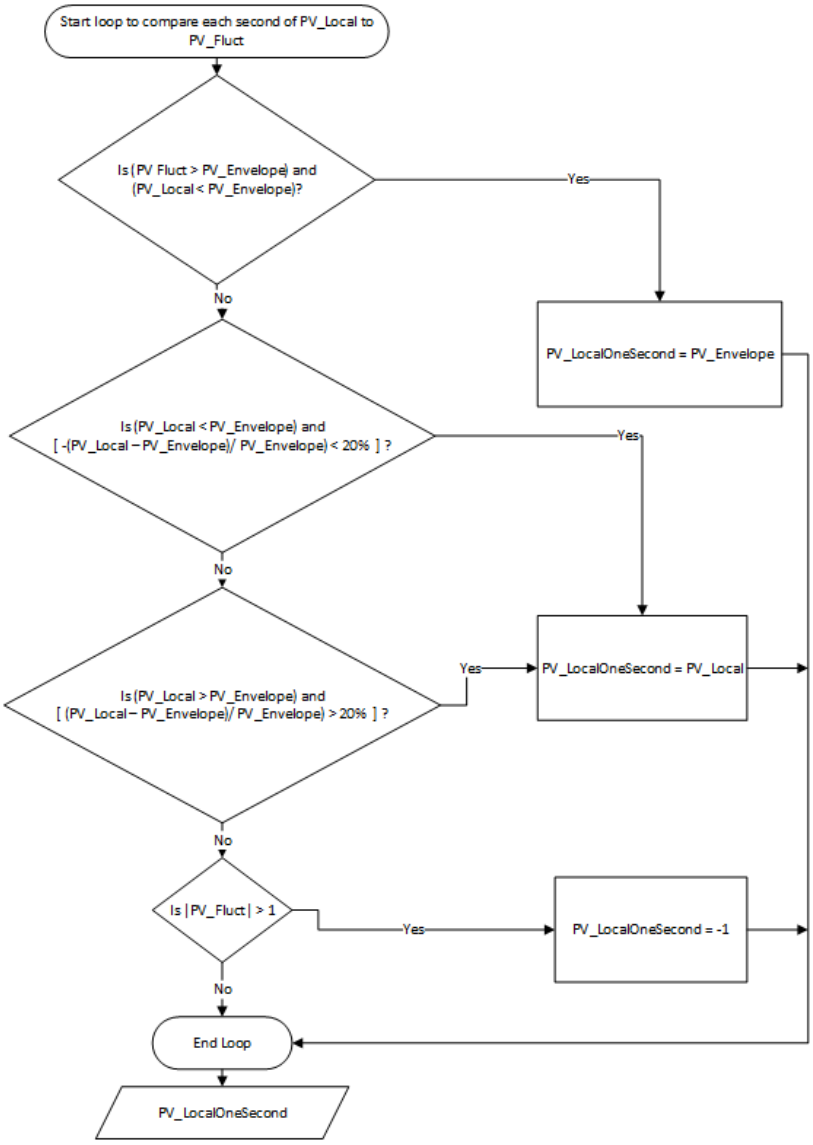

The Salem PV Envelope is used to ensure that these fluctuations do not rise over the maximum solar insolation that can be achieved in Salem. The assumption is that these fluctuations are less geographically dependent than the envelope profile, but they are still

important enough to include in the PV data model in order to help determine proper BESS capacity sizing for a particular feeder. Figure 3.7 shows the imposed fluctuations.

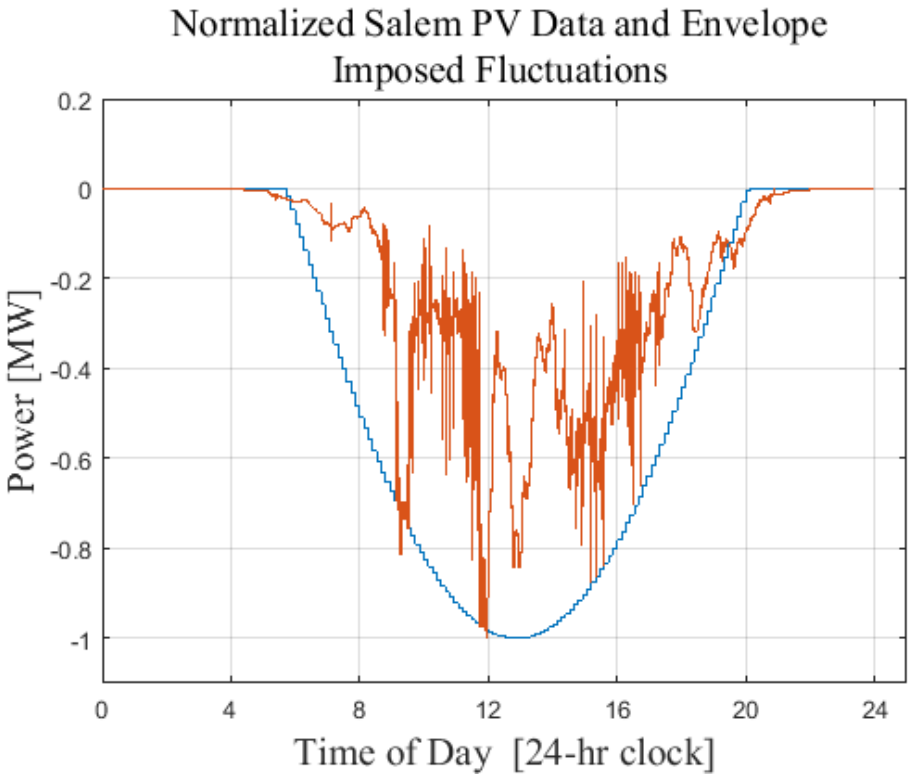

Figure 3.7: This figure shows the PV envelope that was generated by SOLPOS [40], in blue. The PV data collected from the SSPP [39] with the imposed one-second cloud-induced fluctuations provided by Oahu data, shown in red.

Developing a PV profile for every day of the year allows for the data to be combined with the load profile. Prior to combining the PV profile with load data, the profile is scaled to different levels of PV penetration, as a percentage of the feeder size. Equation 3.1 represents the scaling. This step was iterated for 10%-50% penetration in increments of 5%.

$$Salem_{PV\,Scaled} = Salem_{PV\,Fluctuations} \times PV_{Penetration} \times Feeder_{DailyAverage} \tag{3.1}$$

3.1.1.3 Combined PV and Load Data

The normalized load and PV profiles are then combined for 365 days. This is done by subtracting the PV profile from the load data for 365 days, giving the *net load* on the system, $p_{net}(t)$, Equation 3.2. This method is visually represented in Figure 3.8 for a sample day.

$$p_{net}\left(t\right) = p_{load}\left(t\right) - p_{PV}\left(t\right) \tag{3.2}$$

Figure 3.8: Normalized data - in red is Salem PV data with imposed Oahu fluctuations. In blue is normalized Oxford Feeder load profile. In green are the effects of a 35% PV penetration.

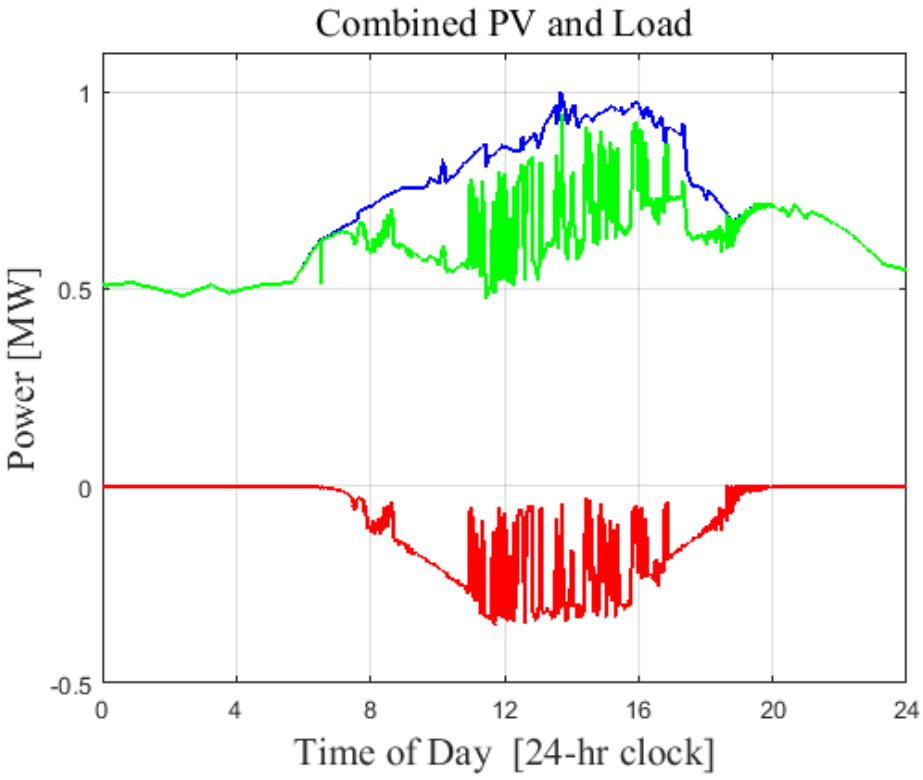

3.1.2 One-Minute Sampling Rate

Both the load profile obtained and the PV generation profile obtained had a sampling rate of one-minute. An assumption was made that one-second granularity in the data is required for a BESS to compensate the cloud-induced fluctuations. To provide a source of comparison, a one-minute sampling rate is also used. The same procedure outlined in Figure 3.2 is used for data preparation of the load and PV generation profiles to provide BESS MW and MWh capacity recommendations.

3.1.2.1 Load Data

Since the sampling rate of both data sets had a one-minute granularity the only procedure performed on the data set is normalization of the data, in order to combine the data.

3.1.2.2 PV Data

Similar to the load data, the only procedure performed was the normalization of the data set. The PV data is then scaled in the same manner as in Section 3.1.1.2 using Equation 3.1 to provide 10%-50% penetration levels in increments of 5%.

3.1.3 Combined PV and Load Data

The normalized load and PV data are then combined, as was done in Section 3.1.1.3, for the different levels of PV penetration.

3.2 Smoothed Desired Feeder Profile

The smoothed desired feeder profile (DFP) is an algorithm that takes the combined PV and load profiles and smooths the data based on a specified window size. A for loop is used in MATLAB to create a best fit curve over the 86,400 second day.

First, *polyfit(X,Y,N)* finds the coefficients of a polynomial *P(X)* of degree *N*, that fits the data *Y* best in a least-squares sense, over the specified window size. A first degree polynomial is used for the smoothed DFP. Then, *polyval(P,X)* returns the value of a polynomial *P* evaluated at *X*. *P* is a vector of length *N+1* whose elements are the coefficients of the polynomial in descending powers.

$$Y = P(1) \times X^N + P(2) \times X^{(N-1)} + ... + P(N) \times X + P(N+1)$$

This algorithm is iterated for the full 86,400 second day, for 365 days. The window sizes were picked in the following manner for the one-second sampling rate: 900 points (pts), 1800 pts, 3600 pts, and 5400 pts, which are 15 minutes (min), 30 min, 60 min, and 90 min window sizes, respectively. For the one-minute sampling rate: 15, 30, 60, and 90 minutes were picked as window sizes.

The following code is used as the function:

```
A = PVplusLoad;                              % Summed PV & Load
C = A';
% Start a for loop to smooth the PV Plus Load over the specified window
% value, parfor is used in this case to utilize parallel processes.
```

```
% Regular  for loop can be used if maximizing speed is not an issue.


% Window sizes:
% 15 min = 900   % 30 min = 1800  % 60 min = 3600 % 90 min = 5400
parfor i = (window + 1): 86400 % max number of points to analyze
                               % 86,400 gets replaced with 1,440
                               % for the one-minute sampling rate
  t = (i-window): i-1;         % Rolling window size decreasing


  extracted_window = C(i-window:i-1);
                       % Extracts window size from transposed PVplusLoad
  B = polyfit(t, extracted_window, 1);
                       % Creates best-fit curve for PV+Load data
                       % 'polyfit(x,y,n)' returns coefficients for
                       % polynomial p(x) of degree n that is a best-fit
                       % in a least-squares sense) for the data
                       % Coefficients in p are in descending powers,
                       % and the length of p is n+1
  A(i,:) = polyval(B,i);
                      % 'polyval(p,x)' returns the value of a polynomial
                      % of degree n evaluated at x
                      % Input argument p is a vector of length n+1,
                      %   with elements that are coefficients in
                      %   descending powers of the polynomial
                      % 'polyval' evaluates B at each element of i
```

```
end                     % loop ends when i > 86400
```

The smoothed profiles are presented in Figure 3.9. It can be observed that the 15 minute smoothed profile follows the combined PV and load the closest, followed by 30 minute, 60 minute, and then 90 minute, respectively.

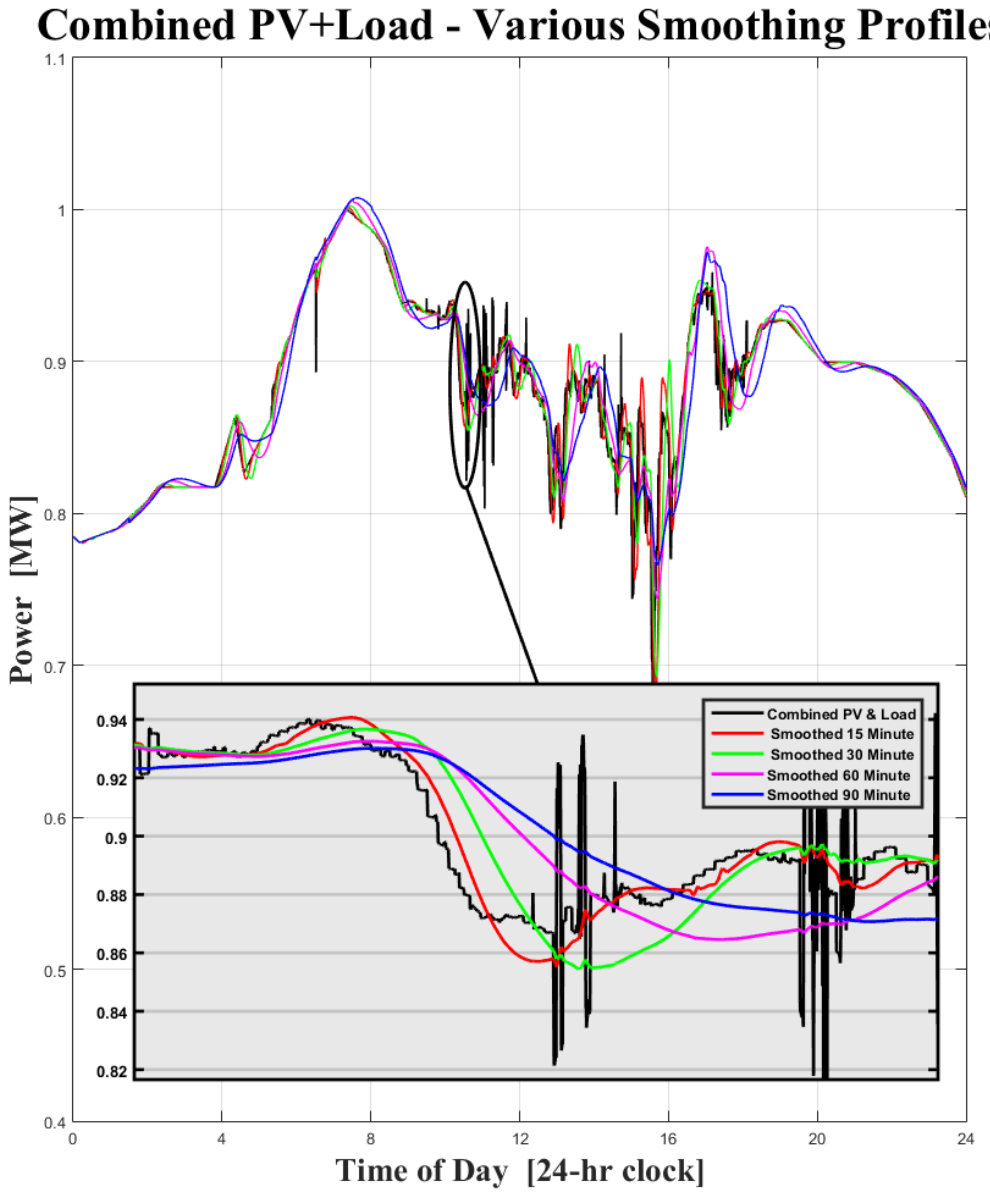

Figure 3.9: Smooth DFP Comparison - This plot shows the combined PV+Load profile *(Black)*, smoothed 15 minute DFP *(Red)*, smoothed 30 minute DFP *(Green)*, smoothed 60 minute DFP *(Magenta)*, smoothed 90 minute DFP *(Blue)*. It provides a comparison of the different variations of the smooth DFP, and shows how it follows the load profile combined with PV generation.

3.3 Power and Energy Requirements

Once the smooth DFP is established, the BESS reference signal, $r_{BESS}\,(t)$, can be calculated; Figure 3.10 shows the reference input signal to the BESS. This is done by subtracting the DFP from the combined PV and Load profiles, as demonstrated in Equation 3.3

$$r_{BESS}\,(t) = p_{DFP} - p_{net}\,(t) \tag{3.3}$$

When loading exceeds the desired feeder profile, the BESS modulates output as an additional generation resource to balance the load. When feeder load falls below the desired feeder profile, the BESS provides extra load, drawing power from the feeder in proportion to the error. Equation 3.4 shows the calculation for the MW capacity for the BESS, $BESS_{MW}$, which is determined by calculating the maximum of the absolute value of the BESS reference signal curve for each day.

$$BESS_{MW} = max(|r_{BESS}\,(t)|) \tag{3.4}$$

The MW capacity is calculated for 365 days using the smoothed DFP, with 15 minute, 30 minute, 60 minute, and 90 minute smoothing window.

The MWh capacity for a BESS is computed using the negative of the BESS reference signal curve, given in Equation 3.5. A cumulative trapezoidal numerical integration is then applied to $r_{BESSneg}$. The peaks are then added to determine energy consumption over a 24 hour period. To obtain MWh the value calculated is then divided by 3,600 for the one-second data set, or 60 for the one minute data.

$$r_{BESSneg}(t) = p_{net}(t) - p_{DFP} \tag{3.5}$$

The MATLAB code describing the process is found below:

```
rBESSneg= PVplusLoad - A;
CumTrapz_MWh=cumtrapz(rBESSneg);
MW24hr=max(CumTrapz_MWh)+abs(min(CumTrapz_MWh));
MWhr=MW24hr/3600; % 3,600 for one second data, 60 for one minute data
```

The MWh capacity is calculated for 365 days using the smoothed DFP, with 15 minute, 30 minute, 60 minute, and 90 minute smoothing window. This is done for different penetration levels to make a recommendation for the MWh capacity requirement to accommodate a given load at different PV penetrations.

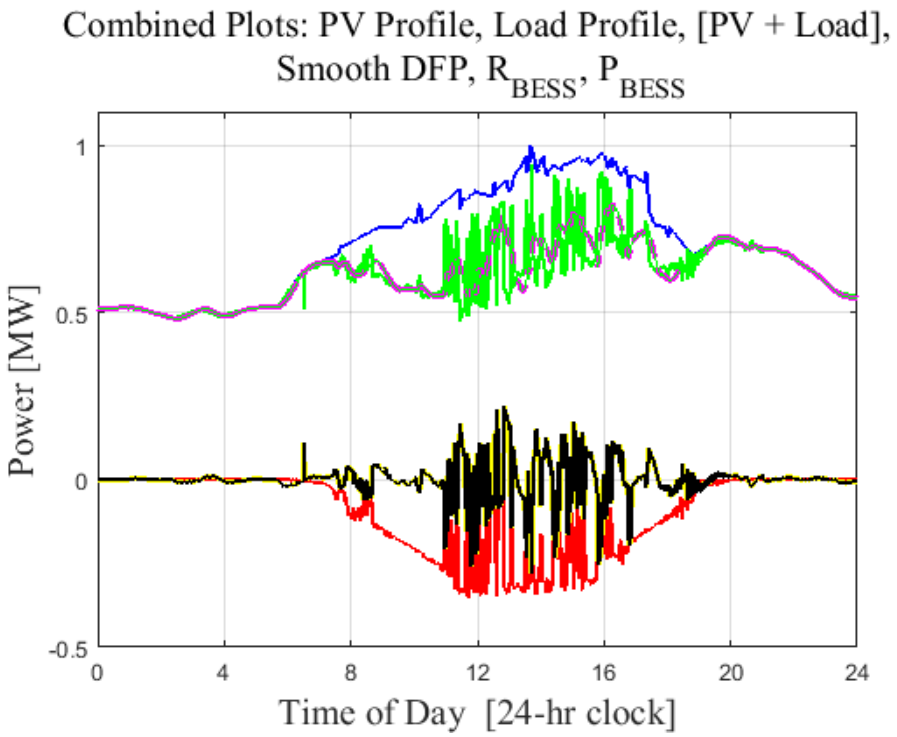

Figure 3.10: Smooth DFP and BESS Response - Shown are load, PV and BESS power profiles for a sample day at a 35% PV penetration level. Key: load (blue), PV (red), net load (green), desired feeder profile (DFP, magenta), BESS reference input signal (yellow) and BESS response (black).

4 Results

In this section, results from a 365 day analysis of BESS energy and capacity requirements for accommodating various levels of PV penetration and smoothed DFPs are presented. Analysis is performed to determine necessary capacities to accommodate the worst case scenarios for a full year on the Oxford-Rural distribution feeder. In a normal distribution a standard deviation is the measure of variation between data points, where the mean is μ. Sigma, σ, is the measure used to quantify the amount of variation in a data set based on the probability of occurrence. The worst case scenario is determined by calculating, $+2\sigma$, of a normal distribution. Which is the point where approximately 95% of the distribution falls within 2 standard deviations of the mean, $\mu \pm 2\sigma$.

This section presents the final results of the variations of the smoothed DFP, alongside the varied PV penetration. The results are presented using a box plot technique, followed by violin plots that show the kernel distribution of the results, and finally a table with MW & MWh capacity recommendations.

4.1 Box Plots

The variance in PV nameplate capacity provided a means for analyzing the necessary megawatt and megawatt-hour requirements for the BESS under differing amounts of renewable penetration. The resulting data were first observed using a box plot and batch

comparison technique. From a box plot, we can pick out the following features of a batch: the location, spread, skewness tail length, and any outlying data points. [41] Figure 4.1 - Figure 4.2 show the generated MW and MWh capacities of the PV penetrations and smoothed DFP, respectively. For this section the y-axes are set to the same limits for the different smoothing scenarios; this is done for ease of comparison.

Figure 4.1 shows the generated box plot results for a 15, 30, and 60 minute smoothed DFP, for power and energy requirements of a BESS. The MW data had a long tail, which indicates skewness in the data set. The MWh data have a considerable amount of outliers.

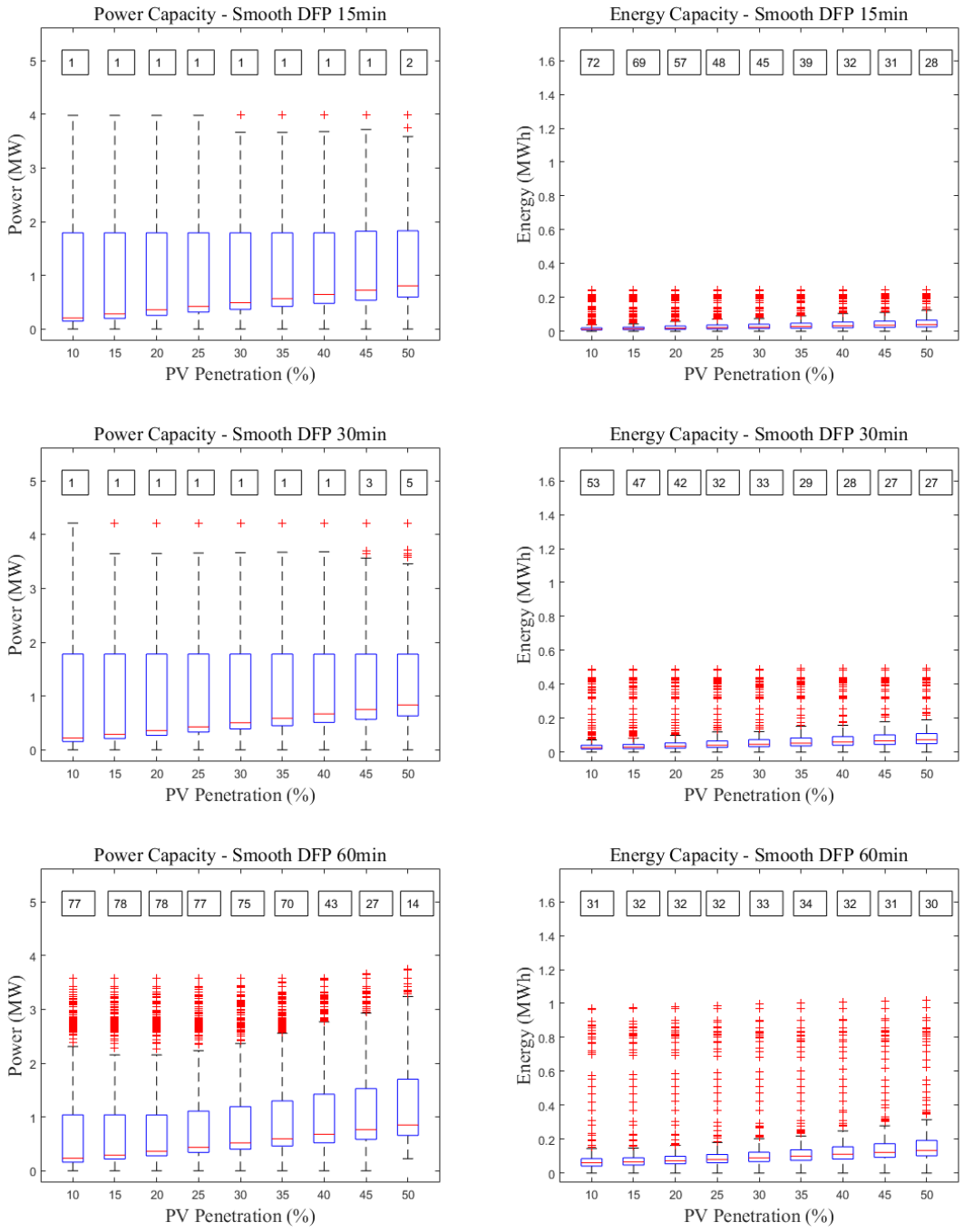

Figure 4.1: Box plots showing MW & MWh capacity for 10%-50% penetration levels using a 15, 30, and 60 minute smooth DFP.

Figure 4.2 shows the generated box plot results for 10%-50% penetration for a 90 minute smoothed DFP.

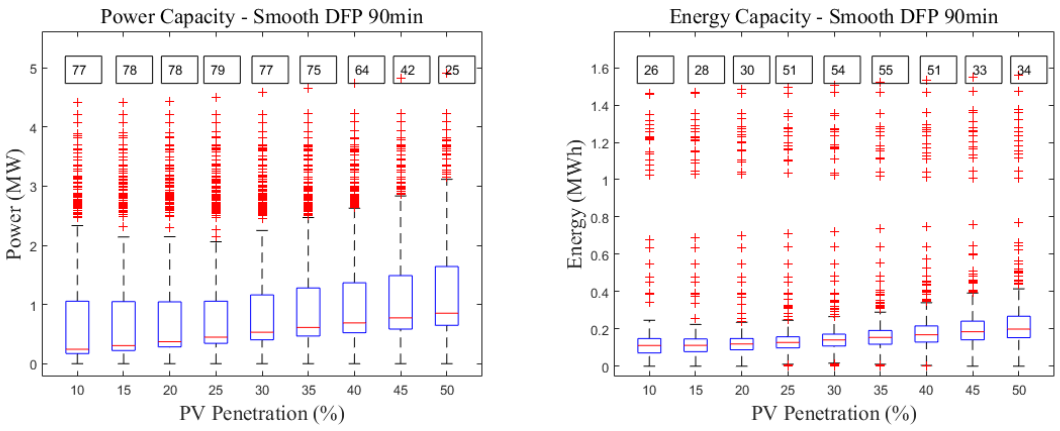

Figure 4.2: Box plots showing normalized MW & MWh capacity for 10%-50% penetration levels using a 90 minute smoothed DFP.

More level of detail is provided in Appendix B with box plots having independent y-axes limits. From the results skewness can be observed, and a considerable amount of outliers. This warrants further investigation.

4.2 Violin Plots

For further investigation, a kernel density plot was used to represent the data. [42] The resulting data has a bi-modal distribution. This is the reason there were so many outliers presented in the box plots. Figure 4.3 shows violin plots representing the kernel distribution of a 15, 30, and 60 minute smoothing function, for 10%-50% PV penetration.

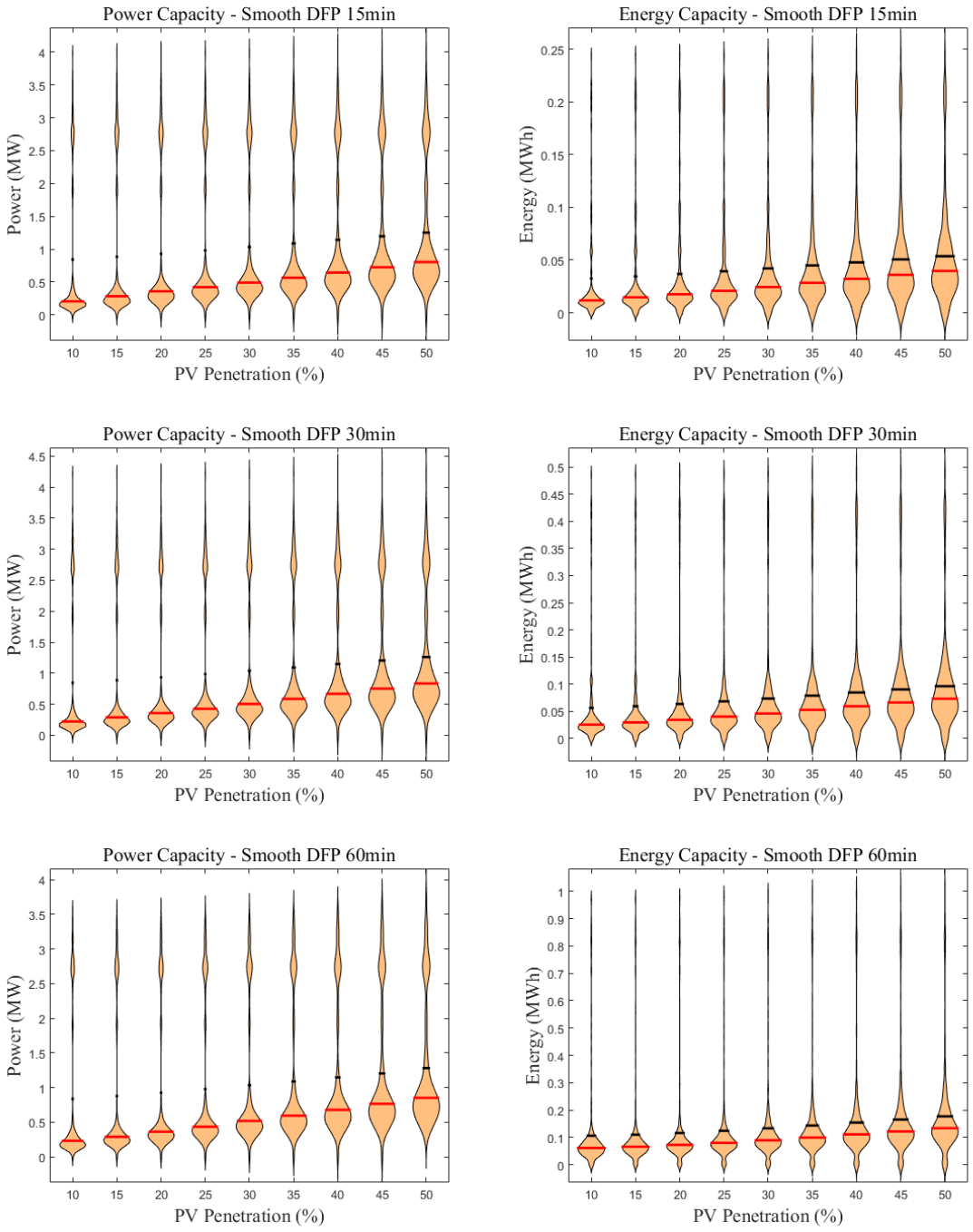

Figure 4.3: Violin plots showing MW & MWh capacity for 10%-50% penetration levels using a 15, 30, and 60 minute smoothed DFP.

Figure 4.4 shows violin plots representing the kernel distribution of a 90 minute smoothing function, for 10%-50% PV penetration.

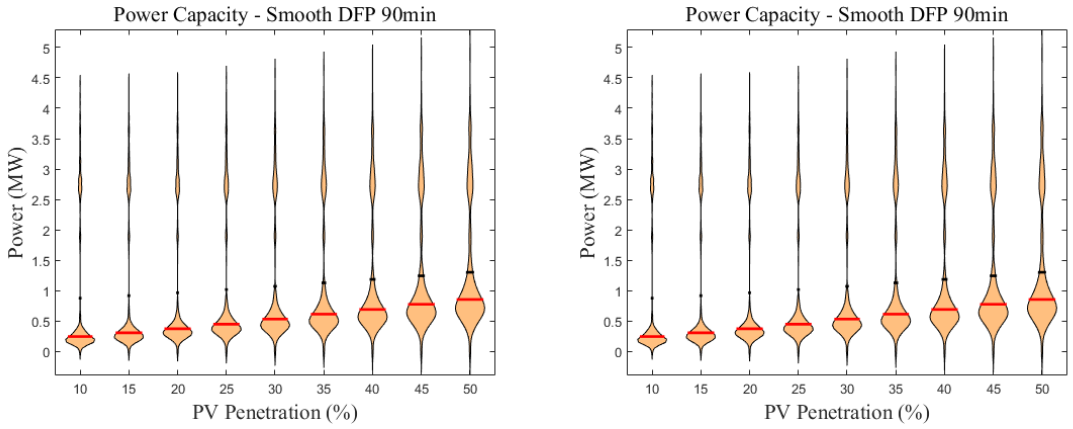

Figure 4.4: Violin plots showing MW & MWh capacity for 10%-50% penetration levels using a 90 minute smoothed DFP.

In order to deal with discrepancies, stratification methods are used to obtain capacity recommendations for sizing the BESS.

4.3 Distribution Fitting

The variables used for stratification are the MW and MWh capacity requirements. The strata are shown in Figure 4.5, which are generated using visualization tools from the MATLAB Distribution fitting toolbox. There are two strata: these are defined by the limits of the bi-modal distribution, of which we are only concerned with confidence intervals from the upper strata. In this section, only two sample plots for MW and MWh are presented. The rest of the plots appear in Appendix C. The bi-modality is further discussed in Section 5.1.

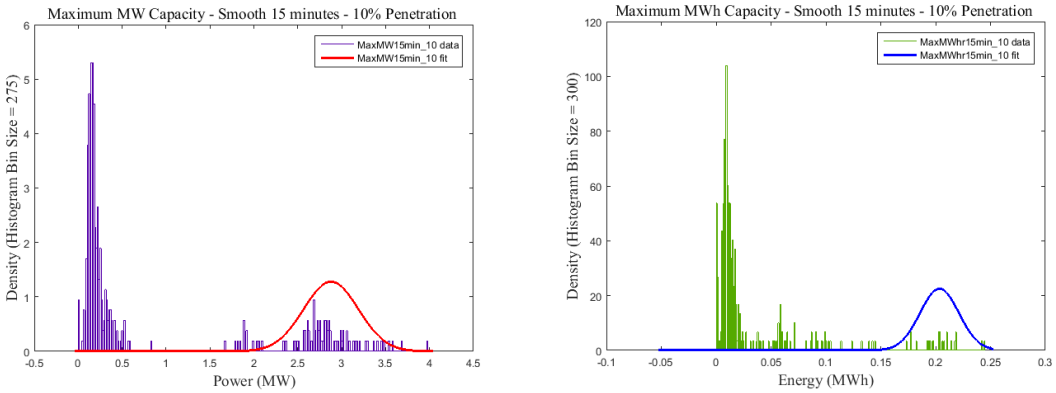

Figure 4.5: Density plots showing MW & MWh capacities with a fitted normal distribution.

4.4 MW & MWh Recommendations

Table 4.1 show the results of the various smoothing versus different levels of PV penetration for a one second granularity.

Table 4.1: Photovoltaic integration by percentage of feeder size - One-Second Granularity - This table shows the power and energy capacity maximums for an annual simulation over various PV penetration levels, indicated as percentages of the feeder size. The results are presents for a Flat DFP, 15 Minute Smooth DFP, 30 Minute Smooth DFP, 60 Minute Smooth DFP, and 90 Min Smooth DFP

BESS Sizing Recommendation - One Second Granularity

PV Nameplate (% of) Feeder Size	Flat DFP		15 Min Smoothing		30 Min Smoothing		60 Min Smoothing		90 Min Smoothing	
	MW Capacity	MWh Capacity	MW Capacity	MWh Capacity	MW Capacity	MWh Capacity	MW Capacity	MWh Capacity	MW Capacity	MWh Capacity
10	3.03	4.41	3.50	0.24	3.55	0.49	3.51	0.98	3.96	1.48
15	3.28	3.87	3.50	0.25	3.56	0.49	3.52	0.98	3.97	1.48
20	3.53	4.08	3.51	0.25	3.57	0.49	3.54	0.99	3.98	1.49
25	3.81	4.70	3.51	0.24	3.58	0.49	3.56	0.99	4.00	1.50
30	4.09	5.76	3.51	0.26	3.59	0.49	3.58	0.99	4.02	1.50
35	4.32	7.07	3.52	0.26	3.60	0.49	3.61	1.00	4.02	1.51
40	4.54	11.81	3.53	0.25	3.62	0.49	3.64	1.00	4.04	1.52
45	4.70	13.15	3.54	0.25	3.66	0.50	3.65	1.01	4.09	1.53
50	4.94	13.85	3.55	0.25	3.74	0.50	3.79	1.02	4.20	1.53

Table 4.2 show the results of one minute granularity of the BESS.

Table 4.2: Photovoltaic integration by percentage of feeder size - One-Minute Granularity - This table shows the power and energy capacity maximums for an annual simulation over various PV penetration levels, indicated as percentages of the feeder size. The results are presents for a Flat DFP, 15 Minute Smooth DFP, 30 Minute Smooth DFP, 60 Minute Smooth DFP, and 90 Min Smooth DFP

BESS Sizing Recommendation - One Minute Granularity

PV Nameplate (% of) Feeder Size	Flat DFP MW Capacity	Flat DFP MWh Capacity	15 Min Smoothing MW Capacity	15 Min Smoothing MWh Capacity	30 Min Smoothing MW Capacity	30 Min Smoothing MWh Capacity	60 Min Smoothing MW Capacity	60 Min Smoothing MWh Capacity	90 Min Smoothing MW Capacity	90 Min Smoothing MWh Capacity
10	3.06	4.16	3.50	0.26	3.66	0.54	3.53	1.14	3.97	1.54
15	3.36	3.98	3.52	.027	3.68	0.54	3.57	1.13	4.01	1.50
20	3.69	4.49	3.54	0.30	3.71	0.56	3.61	1.08	4.03	1.55
25	4.02	5.74	3.52	0.28	3.76	0.56	3.68	1.03	4.04	1.56
30	4.31	6.91	3.53	0.28	3.71	0.56	3.71	1.04	4.06	1.54
35	4.63	7.89	3.56	0.28	3.70	0.56	3.72	1.05	4.16	1.59
40	5.02	10.21	3.58	0.28	3.68	0.55	3.79	1.06	4.16	1.60
45	5.29	11.95	3.58	0.28	3.66	0.54	3.86	1.05	4.01	1.60
50	5.48	13.66	3.64	0.30	3.72	0.55	3.88	1.05	4.04	1.62

To provide a source of comparison, results from the Flat DFP are presented in Table 4.3 for one-second granularity.

Table 4.3: BESS Seasonal Capacity Recommendation for a Flat DFP with One Second Granularity - This table provides the seasonal MW and MWh capacities (Cap) requirements for the various PV penetration levels, indicated as percentages of the feeder size. The one-second granularity is achieved by using Oahu PV data and Salem PV data.

Seasonal BESS Sizing Recommendation - One Second Granularity

PV Nameplate (% of Feeder Size)	SPRING DFP [MW]	SPRING MW Cap	SPRING MWhr Cap	SUMMER DFP [MW]	SUMMER MW Cap	SUMMER MWhr Cap	FALL DFP [MW]	FALL MW Cap	FALL MWhr Cap	WINTER DFP [MW]	WINTER MW Cap	WINTER MWhr Cap	Maximum MW Cap	Maximum MWhr Cap
10%	2.3	0.46	3.1	2.0	0.74	4.1	2.3	0.55	2.9	2.4	0.51	3.3	0.74	4.1
15%	2.3	0.45	2.5	2.0	0.68	3.7	2.2	0.55	2.4	2.4	0.52	3.0	0.68	3.7
20%	2.3	0.45	2.1	1.9	0.63	3.2	2.2	0.56	2.0	2.4	0.54	2.7	0.63	3.2
25%	2.2	0.45	1.7	1.9	0.57	2.9	2.2	0.58	1.9	2.4	0.56	2.5	0.58	2.9
30%	2.2	0.47	1.8	1.8	0.54	2.5	2.1	0.59	2.0	2.3	0.58	2.4	0.59	2.5
35%	2.1	0.49	1.9	1.8	0.50	2.3	2.1	0.61	2.1	2.3	0.60	2.4	0.61	2.4
40%	2.1	0.51	2.1	1.7	0.50	2.1	2.0	0.62	2.3	2.3	0.65	2.5	0.65	2.5
45%	2.0	0.54	2.4	1.7	0.59	2.1	2.0	0.64	2.6	2.3	0.77	2.6	0.77	2.6
50%	2.0	0.60	2.7	1.6	0.67	2.1	1.9	0.68	2.8	2.2	0.89	2.8	0.89	2.8

Table 4.4 provides results for a one-minute granularity of the seasonal analysis.

Table 4.4: BESS Seasonal Capacity Recommendation for a Flat DFP with One-Minute Granularity - This table provides the seasonal MW and MWh capacities (Cap) requirements for various PV penetration levels, indicated as percentages of the feeder size.

Seasonal BESS Sizing Recommendation - One Minute Granularity

PV Nameplate (% of Feeder Size)	SPRING			SUMMER			FALL			WINTER			Maximum	
	DFP [MW]	MW Cap	MWhr Cap	DFP [MW]	MW Cap	MWhr Cap	DFP [MW]	MW Cap	MWhr Cap	DFP [MW]	MW Cap	MWhr Cap	MW Cap	MWhr Cap
10%	2.2	0.52	1.6	2.1	0.66	3.1	1.9	0.49	1.5	2.4	0.63	2.4	0.66	3.1
15%	2.1	0.55	1.1	2.0	0.55	2.4	1.8	0.53	1.6	2.4	0.97	2.4	0.97	2.4
20%	2.0	0.59	2.3	1.9	0.70	2.4	1.7	0.58	2.3	2.4	1.32	2.5	1.32	2.5
25%	1.9	0.82	3.8	1.7	0.94	2.8	1.6	0.81	3.6	2.3	1.67	2.6	1.67	3.8
30%	1.7	1.08	5.2	1.6	1.18	3.9	1.5	1.04	4.8	2.3	2.02	2.7	2.02	5.2
35%	1.6	1.33	6.6	1.5	1.48	5.1	1.4	1.27	6.1	2.3	2.37	2.8	2.37	6.6
40%	1.5	1.59	8.1	1.4	1.78	6.5	1.3	1.50	7.4	2.3	2.72	2.9	2.72	8.7
45%	1.4	1.85	9.5	1.2	2.08	7.9	1.2	1.73	8.8	2.3	3.06	3.0	3.06	9.5
50%	1.3	2.12	11.0	1.1	2.38	9.3	1.1	1.96	10.1	2.2	3.41	3.1	3.41	11.0

A plot of these tables is provided in Figure 4.6, for a visual comparison. The plot shows results for 10%-50% levels of PV penetration and a variance of smoothing profiles for BESS power recommendation for a one minute and one second sampling rate.

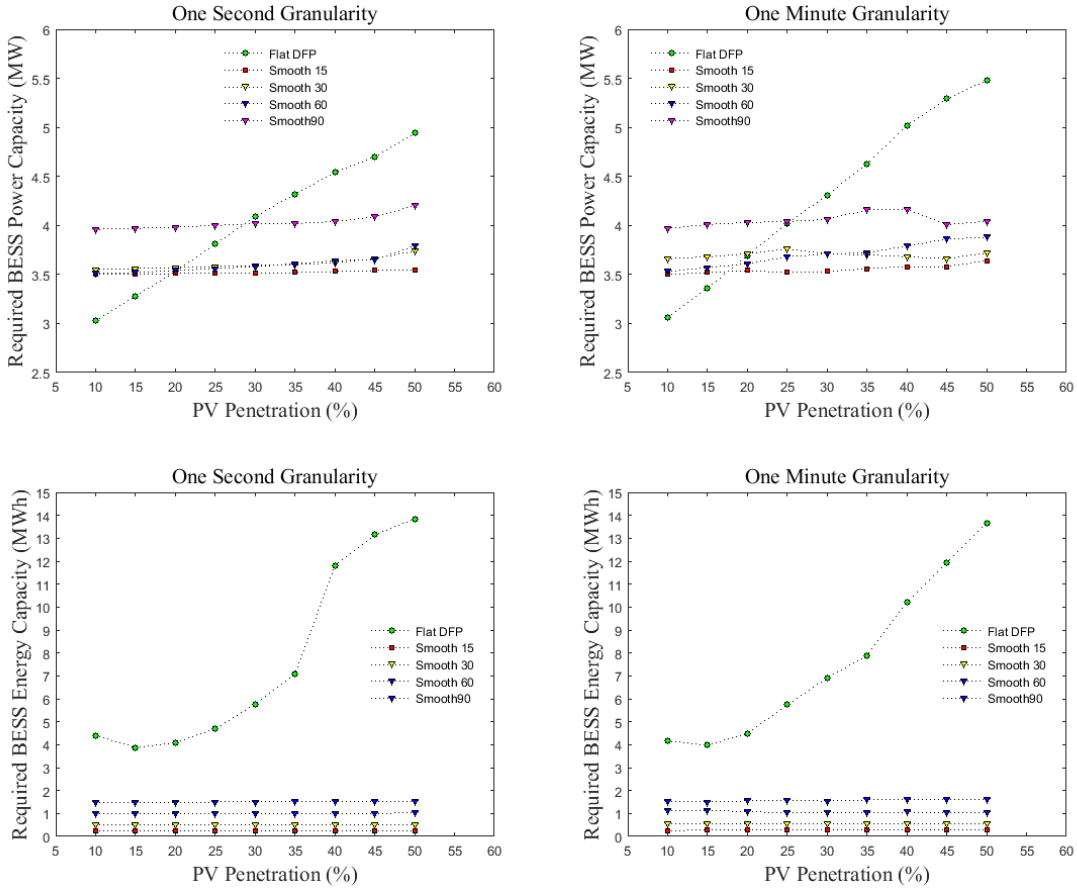

Figure 4.6: PV Penetration VS MW & MWh for various DFPs- These figures provide a comparison of one minute granularity and one second granularity for a Flat DFP, 15, 30, 60, and 90 minute Smooth DFPs.

Table 4.5 and Table 4.6 provide a breakdown of a weekday vs a weekend analysis for the MW and MWh recommendations presented in Tables 4.2.

Table 4.5: Weekend vs Weekday Analysis - One-Min Granularity - Power Capacity (MW)

Weekend vs Weekday Analysis - One Min Granularity - Power Capacity (MW)

PV Nameplate (% of) Feeder Size	Flat DFP		15 Min Smoothing		30 Min Smoothing		60 Min Smoothing		90 Min Smoothing	
	Weekday	Weekend	Weekday	Weekend	Weekday	Weekend	Weekday	Weekend	Weekday	Weekend
10%	252	102	22	11	24	4	26	5	19	3
15%	253	102	24	4	24	4	25	5	19	2
20%	251	102	29	5	25	5	22	3	19	3
25%	255	102	24	2	25	5	19	2	19	3
30%	255	102	23	4	24	4	19	2	19	2
35%	232	189	23	4	35	7	19	2	20	3
40%	222	89	29	6	33	6	20	3	21	3
45%	245	96	39	7	37	9	18	2	20	3
50%	243	96	36	6	37	9	25	5	21	4

Table 4.6: Weekend vs Weekday Analysis - One-Min Granularity - Energy Capacity (MWh)

Weekend vs Weekday Analysis - One Min Granularity - Energy Capacity (MWh)

PV Nameplate (% of) Feeder Size	Flat DFP		15 Min Smoothing		30 Min Smoothing		60 Min Smoothing		90 Min Smoothing	
	Weekday	Weekend	Weekday	Weekend	Weekday	Weekend	Weekday	Weekend	Weekday	Weekend
10%	82	18	67	11	82	18	82	18	82	18
15%	82	18	67	11	82	18	82	18	82	18
20%	83	20	67	11	82	18	82	18	83	18
25%	80	17	66	11	84	20	85	20	68	13
30%	71	16	65	11	100	23	92	22	101	23
35%	71	16	65	13	93	18	73	16	74	16
40%	54	10	76	11	95	19	78	16	85	18
45%	47	8	23	8	118	22	92	18	138	34
50%	36	7	254	102	97	18	134	31	155	39

These results and the comparison of these tables will be further discussed in Section 5.2.

5 Analysis & Discussion

This section discusses the results presented in Section 4. The following sections present discussion of the source of the bi-modal distribution, utilization of boxplots, violin plots, data stratification technique, the final recommendations, and the assumptions that were made.

5.1 Bi-Modal Distribution

Figure 5.1 shows a bar plot of the Oxford-Rural load consumption over 365 days for the year of 2012. This reveals what is believed to be the main source of the bi-modal distribution in the resultant data. It can be observed that this data set has a base load and spikes that occur approximately every five days. It has been confirmed that the source of the spikes in load are weekdays, while the reduced loads occur on the weekends.

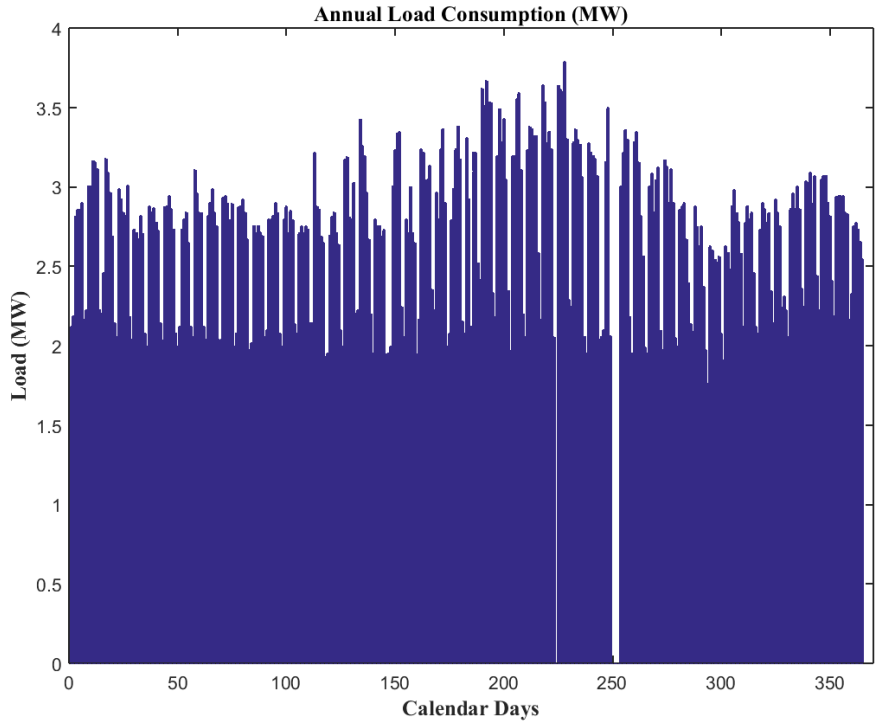

Figure 5.1: Plot showing load consumption on the Oxford-Rural feeder for 366 calendar days. There were days of missing data that create gaps in the load consumption data. In specific, the following days were missing: 221-224, 249-254, and 366.

Figure 5.2 shows a bar plot of the resultant data of the MW capacity for 10% PV penetration for a 15 minute smoothing function. The source of the bi-modal distribution can be observed here as well; there are clearly two different processes occurring. The lower portion of the plot serves to show the base load that is expected throughout the year, while the spikes are more representative of worst case scenario days. The worst case scenario days are occurrences that affect the sizing capacity of the BESS.

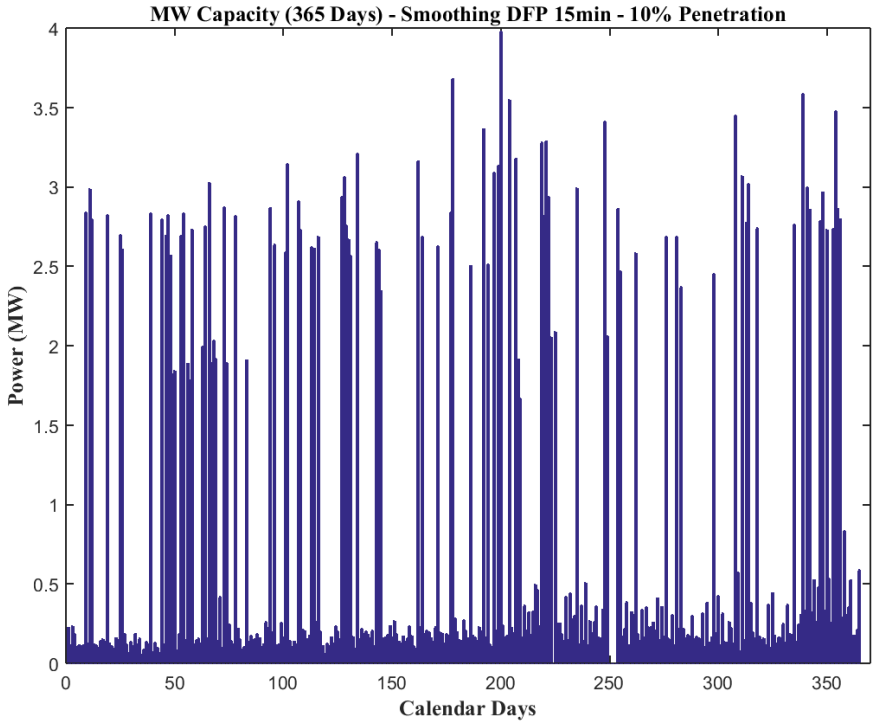

Figure 5.2: Plot showing MW capacity for 365 calendar days for a 10% PV Penetration level using 15 minute smooth DFP. Days with data missing were: 224, 250-253.

Figure 5.3 shows a bar plot of the resultant data of the energy capacity for 50% PV penetration for a 15 minute smoothing function. The source of the bi-modal distribution can be observed here as well, there are clearly two different processes occurring. The lower portion of the plot serves to show the base load that is expected throughout the year, while the spike are more representative of worst case scenario days.

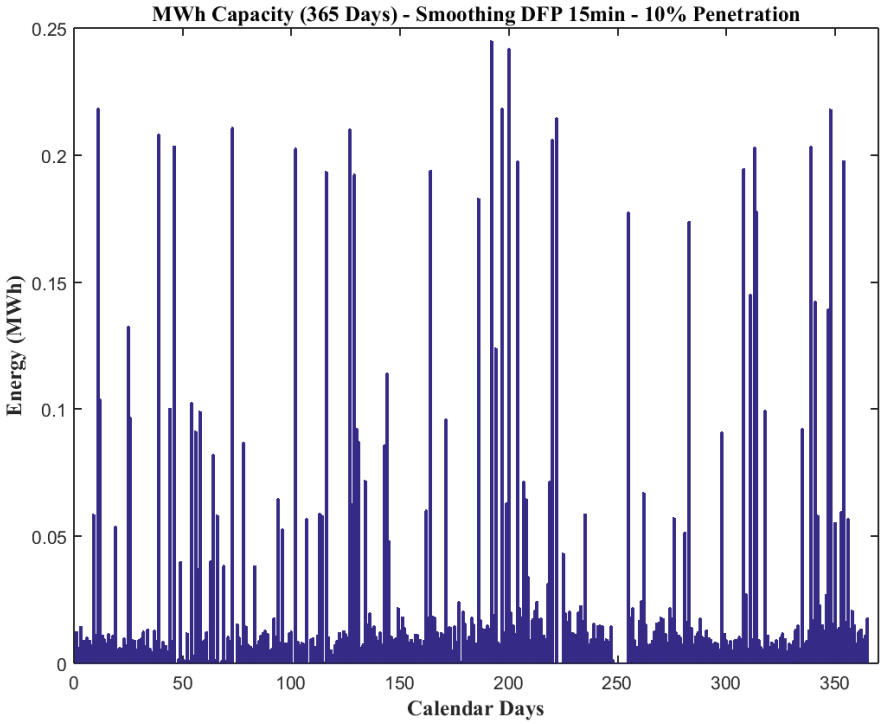

Figure 5.3: Plot showing MWh capacity for 365 calendar days for a 50% PV Penetration level using 15 minute smooth DFP. Days with data missing were: 67, 74, 101, 221, 223, 224, 249-254.

5.2 Flat DFP VS Smooth DFP

Table 4.1 provides the values established for energy and power capacity for different variations of the smoothing function over 10%-50% PV penetration levels. As a comparison, Table 4.3 is provided to compare the annual study to the seasonal study. From these tables, it can be deduced that the energy requirements go down by more than a factor of 10 when the smoothing function is utilized in comparison to the flat feeder profile. This then begs the question of why the power capacities are higher. The reason the power requirements are higher is that in an annual study the worst case scenarios can be truly observed, while there was a limiting factor of the four representative days in the seasonal study. Figure 5.2 shows

that there were cases where the MW capacity stayed within the operating base, and did not spike; which brings us to the conclusion that the representative days from the seasonal study must have fallen within that base.

Figures 4.6 show the plots of the of the results for 10%-50% levels of PV penetration and a variance of smoothing profiles for a one-minute and one-second granularity. It should be noted that for the MW comparison, the data appears to be linearly increasing for the various smoothing profiles and that there is an overlap between the 30 minute smooth DFP, and the 60 minute smooth DFP. The cause of the overlap occurs due to the smoothing algorithm. The smoothing algorithm utilizes poly-fitting to achieve the smoothing, which may cause the discrepancy in overlap. Overall, there were no major differences between one-second and one-minute granularity analysis.

Figure 5.4 shows the BESS capability of providing firming for a sample day with cloud-induced fluctuations. The blue line is the combined PV generation output (at 50% PV penetration level) and load profiles. Shown in green is the smoothed desired feeder profile, and in red is the reference signal to the BESS. When the reference signal falls below zero it indicates the BESS is used as an extra generation resource to mitigate for fluctuations. On the other hand, when the reference signal goes above zero it indicates that the BESS can be used to store the extra generated capacity.

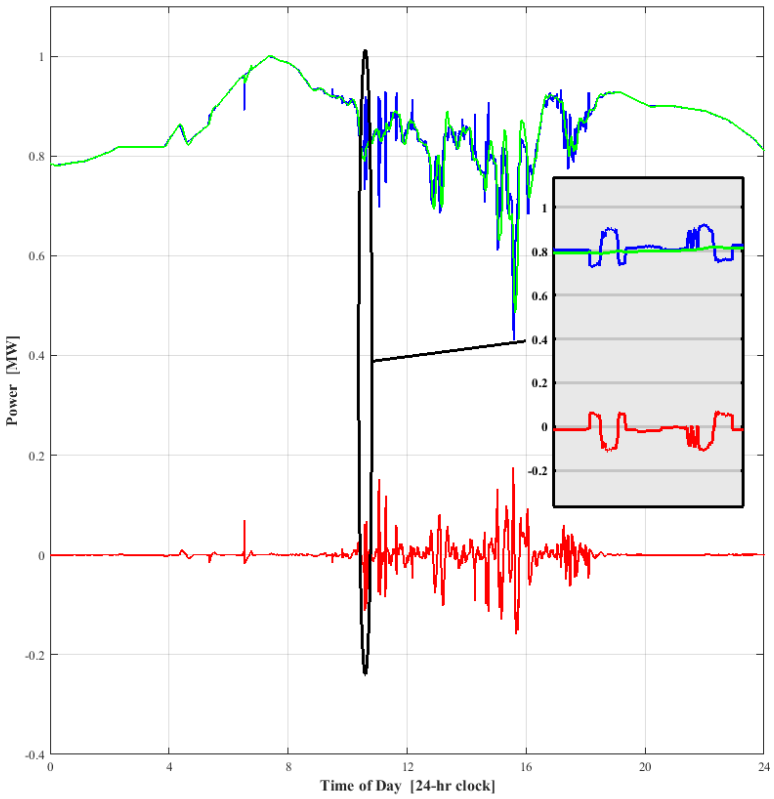

Figure 5.4: BESS Firming Capability - This plot shows a BESS capability of providing firming. Shown (in blue) is the Combined Load and PV for a sample day. Shown (in green) is the smoothed desired feeder profile. Shown (in red) is the reference signal to the BESS to accommodate for fluctuations.

Table 4.5 and Table 4.6 provide a breakdown of a weekday vs a weekend analysis for the MW and MWh, respectively. Recommendations presented shows that the worst case scenarios for the recommended BESS capacity fall within weekdays, which are the days that the utility would be most concerned with covering.

5.3 Assumptions

This section discuses the assumptions made to proceed with the data processing, the outcomes of these assumptions, and validation for the method used for the data stratification procedure.

5.3.1 Missing Data

Initially when the data were processed, there were a few discrepancies that were not dealt with in the most appropriate fashion, according to Pearson. [37] The collected Salem PV data for the year had days missing; these values were asserted as zeros, and were not changed. According to Pearson, this data is considered "non-ignorable missing data", and the missing days should be assumed close to those days preceding it or the days that follow it. Computationally, these days appeared as outliers in the system, since we know that there was PV generation occurring that day, and that the error is a system measurement failure. This could lead to significant biases in the analysis of the results. Missing data is an extremely common anomaly in large data-sets. Corresponding values that should be present in a data-set, but are absent for various reasons. A common source of missing data is measurement system failures, which can occur in either manual or automated data collection systems. Non-ignorable missing data generally correspond to systematically missing data values from a data-set. The consequences are more severe, since it often introduces significant biases into our analysis results. However, in this case the missing data that were assumed as zero created a skew of outlying data that appeared at zero.

5.3.2 Misalignment

As noted previously, the data collected was from a span of several years; Salem PV profile (2014), Oahu PV profile (2010-2011), and the Oxford load profile (2012). It so happens that 2012 was a leap year, providing 366 days of data while the other data sets contained 365 days of data. Therefore, the final day from 2012 was omitted from the analysis.

The Oxford data contains more than one process as shown in Figure 5.1. A quick visual frequency analysis shows that the data have 52 peaks associated with discrepancy between weekend and weekdays. When a kernel probability distribution is plotted, the result is a bi-modal distribution, as was shown in Figure 4.3.

The weekdays have been associated with more energy consumption than the weekends. This derives from the understanding that there are less industrial processes operating during the weekend; Oregon's industrial energy consumption makes up nearly 26% of the overall energy generated. [34]

When an analytical comparison is done between the days associated with higher energy consumption, it was found that these days correlated with weekdays, therefore the deduction was correct. However, the process utilized data from several years; this creates misalignment in the final results. While there is still a bi-modal distribution occurring, there was no perseverance in which days were weekends or weekdays. Recommendations for future studies would be to match load data, and PV data from the same year in order to get meticulous sizing recommendations, along with performing a weekday study independently from weekends. This being said, no conspicuous reason has been presented that there is

lapse in the analysis of the results.

5.3.3 Outliers

It is important to emphasize that undetected data anomalies can arise from gross measurement errors and other highly unreliable sources, and that the effects of these anomalies can be catastrophic. However, in this case, the outliers have been identified to be occurring as a result of an underlying process.

5.3.4 Data Stratification

In order to make a statistically valid recommendation for battery energy and power capacities, part of the data were eliminated from the data set. The battery power and energy recommendations are geared towards worst case scenarios. Therefore, including data from the lower strata would be redundant because those cases would be covered by the recommendation for battery size during worst case scenarios. These worst case scenarios are associated with weekdays. The visual representation showing the data that was considered as part of this analysis is provided in Appendix C.

5.4 Recommendations

For the reproducibility of this work, I recommend that annual load and PV profiles collected be from the same year. This would then allow further analysis into the diurnal effects. I also recommend, to not ignore missing data due to errors in data collection methods. The use of the previous day or the following day would make a valid assumption, and would produce

less skewness in results; in reality we know that there was energy consumed and energy produced those days, therefore, omitting those days from the study is not the best course of action. A one-minute sampling rate was found to be sufficient in modeling the effects of cloud-induced fluctuations, and BESS capacity recommendations did not vary greatly.

6 Conclusion

As society continually grows and expands the demand for power and energy consumption grows as well. With the technological advances being made, renewable energy is a significant part of the electric grid infrastructure. With any growth opportunity there can be positive and adverse effects. This thesis aims to provide a solution for mitigating electrical grid issues that arise with high levels of PV penetration on a distribution feeder.

The proposed solution to mitigate the negative effects of PV generation is to utilize a BESS, regulated using a smooth feeder profile. The methodology described in this thesis aims to provide insight on providing the BESS with a control system, Figure 2.1, that is able to provide firming and shaping to the electric grid. Figure 2.2 showed the response of the PID-compensated control system, and indicates that the proposed control system has sufficient transient response to charge and discharge the BESS in response to variations in load and PV generation. [16] Figure 3.9 showed the differences in smooth DFPs, and the ability to follow the combined load. Figure 5.4 showed insight on how the BESS can be utilized to provide firming capability, by providing a reference signal to the BESS.

The BESS should be sized appropriately for the distribution feeder. This thesis provides the methodology for sizing MW and MWh capacities for the BESS. The study performs a year-long analysis on existing load profiles from previously collected data, and a PV profile to provide a reference signal to the BESS that is able to provide firming of power.

This method is demonstrated for different percentages of PV penetration associated with the distribution feeder, as well as variations of the smoothed feeder profile as reference to the BESS. This method is conducted using a one-minute sampling rate and a one second sampling rate. Statistical analytical methods are then used to determine appropriate sizing to accommodate the stated high PV penetration levels for worst case scenarios.

With the utilization of different lengths of smoothing DFPs, energy and power capacities of the BESS varied between 3.50 MW - 4 MW, and 0.24MWh -1.53 MWh, respectively. These values are sufficient to accommodate high levels of PV penetration on the Oxford-Rural distribution feeder, as was presented in Table 4.1. Figure 4.6 shows the comparison of a one-minute sampling rate to that of one-second, it was concluded that the one-minute sampling rate is sufficient to provide the level of detail necessary to make recommendations for BESS capacity requirements. This method is applicable to any distribution feeder to provide BESS energy and storage capacity as long as the necessary load profile and PV profile are present.

Bibliography

[1] Roger Peters and Cherise Burda. The basics on base load: Meeting Ontario's base load electricity demand with renewable power source. Technical report, Pembina Institute, 2007.

[2] Cristina L. Archer and Mark Z. Jacobson. Supplying baseload power and reducing transmission requirements by interconnecting wind farms. *Journal of Applied Meteorology and Climatology*, 46(11):1701–1717, 2007.

[3] Chris Nelder. Why baseload power is doomed. `http://www.zdnet.com/article/why-baseload-power-is-doomed/`. Accessed: 2016-03-28.

[4] George Pratt Shultz and Robert C. Armstrong. *Game Changers Energy on the Move*. Hoover Institution Press, 2014.

[5] E. Bitar, R. Rajagopal, P. Khargonekar, K. Poolla, and P. Varaiya. Bringing wind energy to market. *IEEE Transactions on Power Systems*, 27(3):1225–1235, 2012.

[6] E. Ela and D. Edelson. Participation of wind power in LMP-based energy markets. *IEEE Transactions on Sustainable Energy*, 3(4):777–783, 2012.

[7] D. Lew, G. Brinkman, E. Ibanez, M. Hummon, B. M. Hodge, M. Heaney, and J. King. Sub-hourly impacts of high solar penetrations in the western united states. In *2nd International Workshop on Integration of Solar Power in Power Systems Proceedings, Lisbon, Portugal*, 2012.

[8] W. Jewell and R. Ramakumar. The effects of moving clouds on electric utilities with dispersed photovoltaic generation. *IEEE Transactions on Energy Conversion*, EC-2(4):570–576, 1987.

[9] G. Liu and K. Tomsovic. Quantifying spinning reserve in systems with significant wind power penetration. *IEEE Transactions on Power System*, 27(4):2385–2389, 2012.

[10] B.C. Ummels, M. Gibescu, E. Pelgrum, W.L. Kling, and A.J. Brand. Impacts of wind power on thermal generation unit commitment and dispatch. *Energy Conversion, IEEE Transactions on*, 22(1):44–51, 2007.

[11] D. Picault, B. Raison, S. Bacha, J. Aguilera, and J. De La Casa. Changing photovoltaic array interconnections to reduce mismatch losses: a case study. In *Environment and Electrical Engineering (EEEIC), 2010 9th International Conference on*, pages 37–40, 2010.

[12] M. Obi, R. Bass, and S.M. Jensen. Levelized cost of energy for energy storage systems. In *Energy Policy (submitted)*, 2015.

[13] North American Electric Reliability Corporation. Glossary of terms used in NERC reliability standards. `http://www.nerc.com/files/glossary_of_terms.pdf`. Accessed: 2016-04-20.

[14] S. Abdelrazek and S. Kamalasadan. Integrated control of battery energy storage management system considering PV capacity firming and energy time shift applications. In *2014 IEEE Industry Applications Society Annual Meeting*, pages 1–7, 2014.

[15] M. H. Coddington, D. Baca, B. D. Kroposki, and T. Basso. Deploying high penetration photovoltaic systems; a case study. In *2011 37th IEEE Photovoltaic Specialists Conference (PVSC)*, pages 002594–002599, 2016.

[16] R. Bass, S. Munden, T. Huang, A. Hamadah, E. McCallum, and P. Nounkwa. Salem Battery Energy Storage System: Plant Modeling & Compensation - Part II. Technical report, Portland State University, Portland, OR, June 2014.

[17] Eric Hirst and Brendan Kirby. Defining intra-and interhour load swings. *Power Systems, IEEE Transactions on*, 13(4):1379–1385, 1998.

[18] A. Oudalov, R. Cherkaoui, and A. Beguin. Sizing and optimal operation of battery energy storage system for peak shaving application. In *Power Tech, 2007 IEEE Lausanne*, pages 621–625, 2007-07.

[19] Jim Eyer and Garth Corey. Energy storage for the electricity grid: Benefits and market potential assessment guide. *Sandia National Laboratories*, 20(10):5, 2010.

[20] C.D Rahn and C.Y. Wang. *Battery Systems Engineering*. Wiley, 2013.

[21] Y. Yang, H. Li, A. Aichhorn, J. Zheng, and M. Greenleaf. Sizing strategy of distributed battery storage system with high penetration of photovoltaic for voltage regulation and peak load shaving. *IEEE Transactions on Smart Grid*, 5(2):982–991, 2014.

[22] Gilbert M. Masters. *Renewable and Efficient Electric Power Systems*. Wiley, 2005.

[23] Roger Messenger and Jerry Ventre. *Photovoltaic Systems Engineering*. CRC Press, 2000.

[24] R. Bass, J. Aguilar, J. Carr, and W. Murar. Salem Battery Energy Storage System: BESS MW & MWh Capacity for Maximizing PV Penetration. Technical report, Portland State University, Portland, OR, 2015.

[25] Katsuhiko Ogata. *Modern Control Engineering*. Prentice Hall, 2010.

[26] R. Bass, J. Carr, J. Aguilar, and K. Whitener. Determining the power and energy capacity of a battery energy storage system to accommodate high photovoltaic penetration on a distribution feeder. In *IEEE Power and Energy Technology Systems Journal (submitted)*, 2015.

[27] K. Whitener and *et al.* Salem smart power project acceptance test documentation and results. Technical report, Portland General Electric, August 2014.

[28] H. Zheng, S. Li, C. Zang, and W. Zheng. Coordinated control for grid integration of PV array, battery storage, and supercapacitor. In *2013 IEEE Power Energy Society General Meeting*, pages 1–5, 2013.

[29] N. Jayasekara, M. A. S. Masoum, and P. Wolfs. Optimal power management for LV distribution feeders with finely distributed PV and co-located storage. In *2013 IEEE Power Energy Society General Meeting*, pages 1–5, 2013-07.

[30] Heath Gurganus. Battery energy storage systems to mitigate the variability of photovoltaic power generation. Master's thesis, Portland State University, December 2013.

[31] Adarsh Nagarajan. *Model Development and Analysis of Distribution Feeders with High Penetration of PV Generation Resources*. PhD thesis, Arizona State University, May 2015.

[32] W. A. Omran, M. Kazerani, and M. M. A. Salama. Investigation of methods for reduction of power fluctuations generated from large grid-connected photovoltaic systems. *IEEE Transactions on Energy Conversion*, 26(1):318–327, 2011.

[33] J. H. Teng, S. W. Luan, D. J. Lee, and Y. Q. Huang. Optimal charging/discharging scheduling of battery storage systems for distribution systems interconnected with sizeable PV generation systems. *IEEE Transactions on Power Systems*, 28(2):1425–1433, 2013-05.

[34] U.S. EIA. U.s. energy information administration - EIA - independent statistics and analysis, 2016. `http://www.eia.gov/state/?sid=OR#tabs-2`. Accessed: 2016-04-14.

[35] Robert S. Reichard. *The Numbers Game, Uses and Abuses of Managerial Statistics*. McGraw-Hill Book Co., Chichester, West Sussex, 1972.

[36] Carl-Erik Särndal. *Model assisted survey sampling*. Springer series in statistics. New York : Springer-Verlag, 1992.

[37] Ronald K . Pearson. *Mining imperfect data : dealing with contamination and incomplete records*. Philadelphia : Society for Industrial and Applied Mathematics, 2005.

[38] S. Wilcox and A. Andreas. NREL Report No. DA-5500-56497. *Solar Resource & Meteorological Assessment Project (SOLRMAP): Rotating Shadowband Radiometer (RSR), Kalaeloa Oahu, Hawaii (Data)*, 2010.

[39] Frank Vignola, Rich Kessler, and Josh Peterson. Srml station: Salem, or (pv). *University of Oregon: Solar Radiation Monitoring Laboratory*, 2015.

[40] A. Andreas. Measurement and Instrumentation Data Center (NREL MIDC) Solar Position and Intensity (SOLPOS). *National Renewable Energy Laboratory*, 2015.

[41] David C. Hoaglin, David C. Hoaglin, Frederick Mosteller, and John Wilder Tukey. *Understanding robust and exploratory data analysis* -. Wiley, New York, 1983.

[42] H. Hoffmann, 2015. violin.m - Simple violin plot using matlab default kernel density estimation. INRES (University of Bonn), Katzenburgweg 5, 53115 Germany. hhoffmann@uni-bonn.de `http://www.mathworks.com/matlabcentral/fileexchange/45134-violin-plot`.

Appendix A: Code Repository

The codes used will be provided as part of a github repository.

`https://github.com/osamammansour/BESS-Thesis`

Appendix B: Box Plots

This section contains the same box plots provided in Section 4.1 with defined y-limits. This is done in order to provide further visual depth in the data sets. Figure B.1 shows the generated box plot results for 10%-50% PV penetration for a 15 minute smoothed DFP. The MW data had a long tail, which indicates skewness in the data set. The MWh data had a considerable amount of outliers.

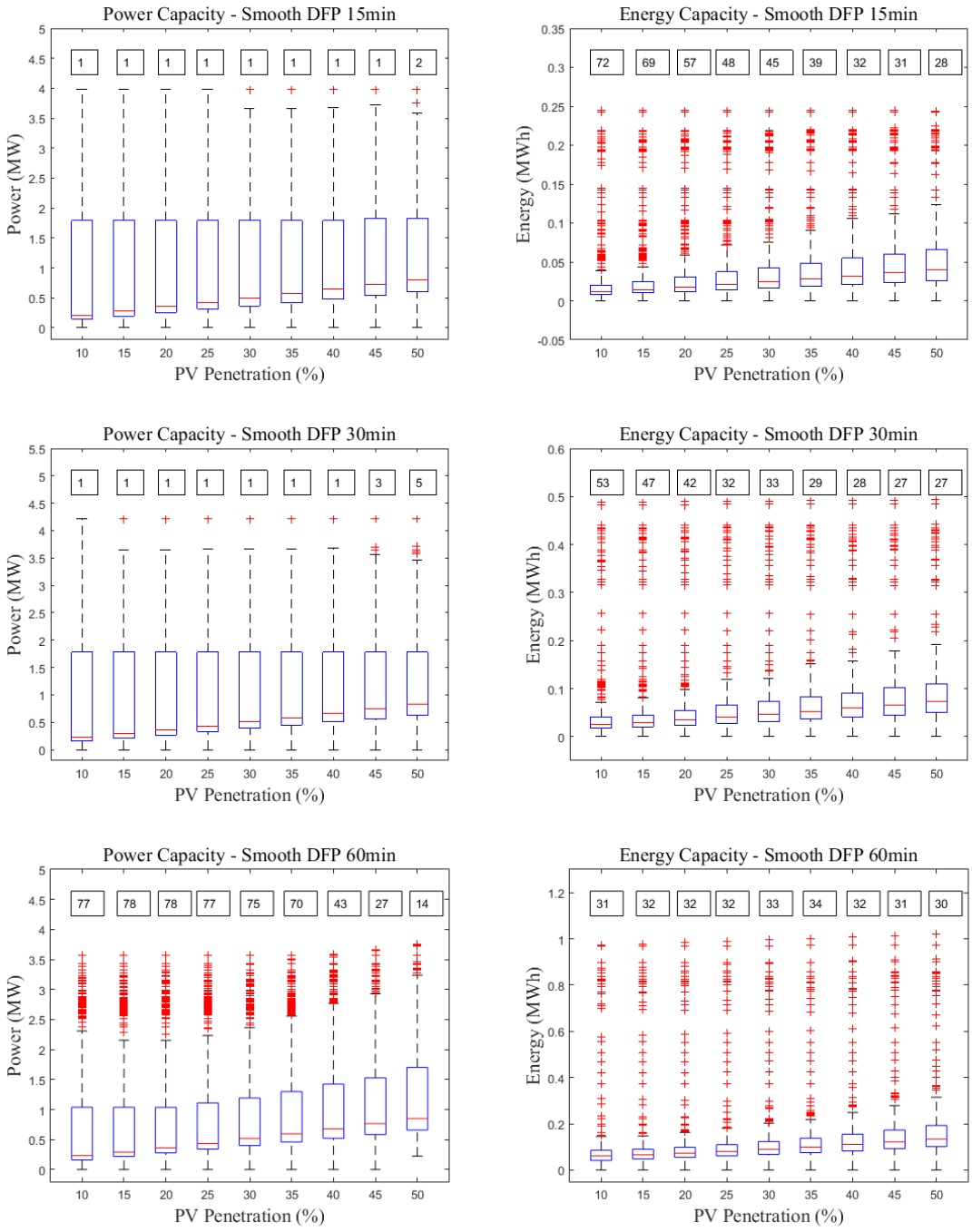

Figure B.1: Box plots showing MW & MWh capacity for 10%-50% penetration levels using a 15, 30, and 60 minute smoothed DFP.

Figure B.2 shows the generated box plot results for 10%-50% penetration for a 90 minute

smoothed DFP. Similar to the 60 minute of smoothing, both MW and MWh capacities have a considerable amount of outliers.

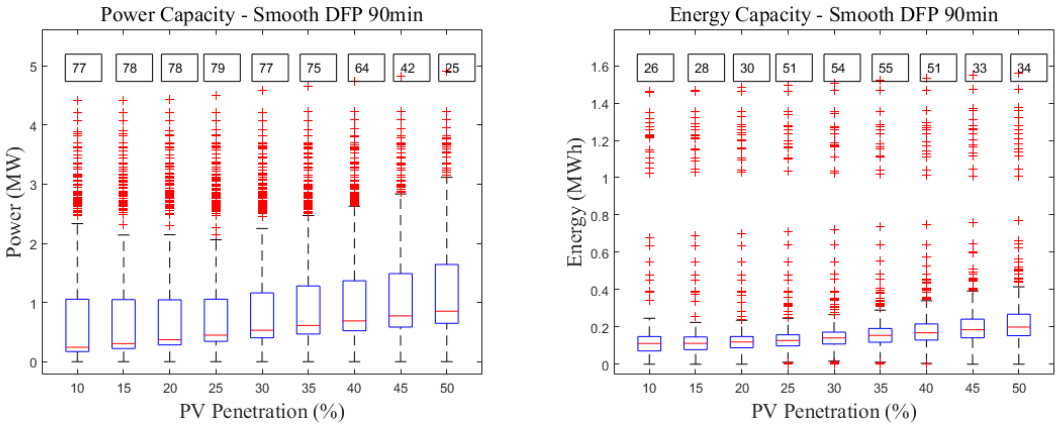

Figure B.2: Box plots showing normalized MW & MWh capacity for 10%-50% penetration levels using a 90 minute smoothed DFP.

Appendix C: Distribution Fitting

This section contains the plots showing a visual representation of the data stratification process for MW & MWh recommended capacities. Figure C.1 shows the plots for 15 minute smoothing for 10%-35% PV penetration MW Capacity.

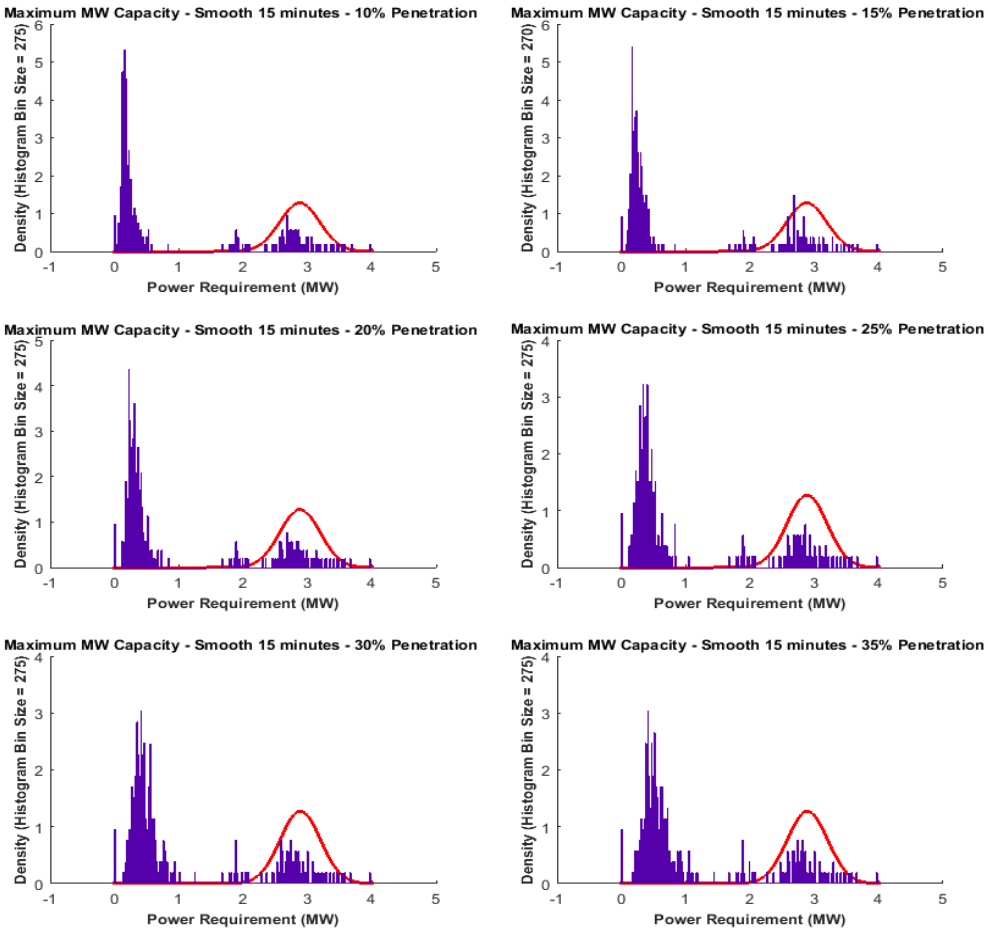

Figure C.1: Fitted Distribution 15 minute smoothing 10%-35% MW Capacity

Figure C.2 shows the plots for 15 minute smoothing for 40%-50% PV penetration MW Capacity, and 10%-20% PV Penetration MWh capacity.

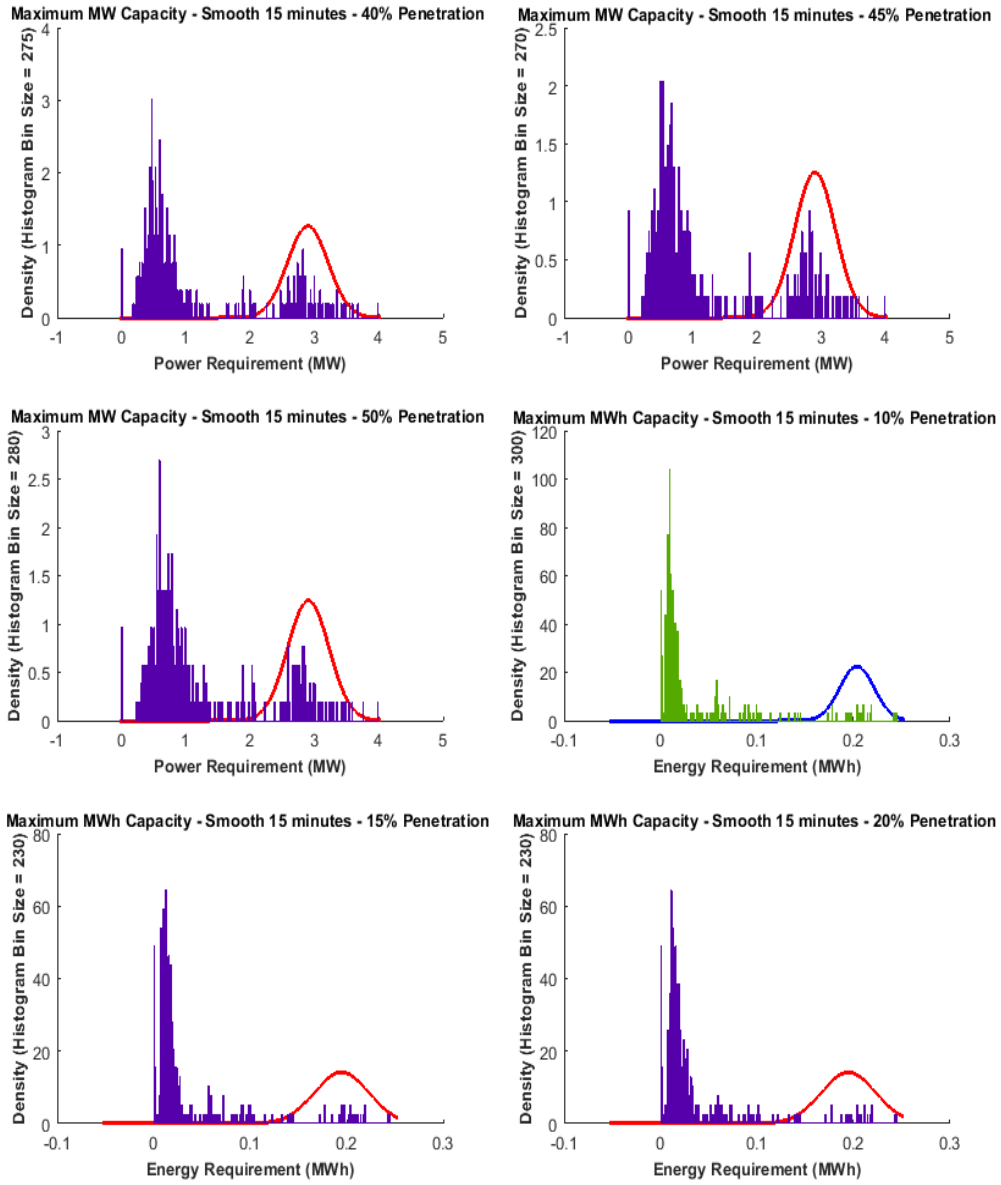

Figure C.2: Fitted Distribution 15 minute smoothing for 40%-50% PV penetration for MW Capacity, and 10%-20% PV Penetration MWh capacity.

Figure C.3 shows the plots for 15 minute smoothing for 25%-50% PV penetration MWh Capacity.

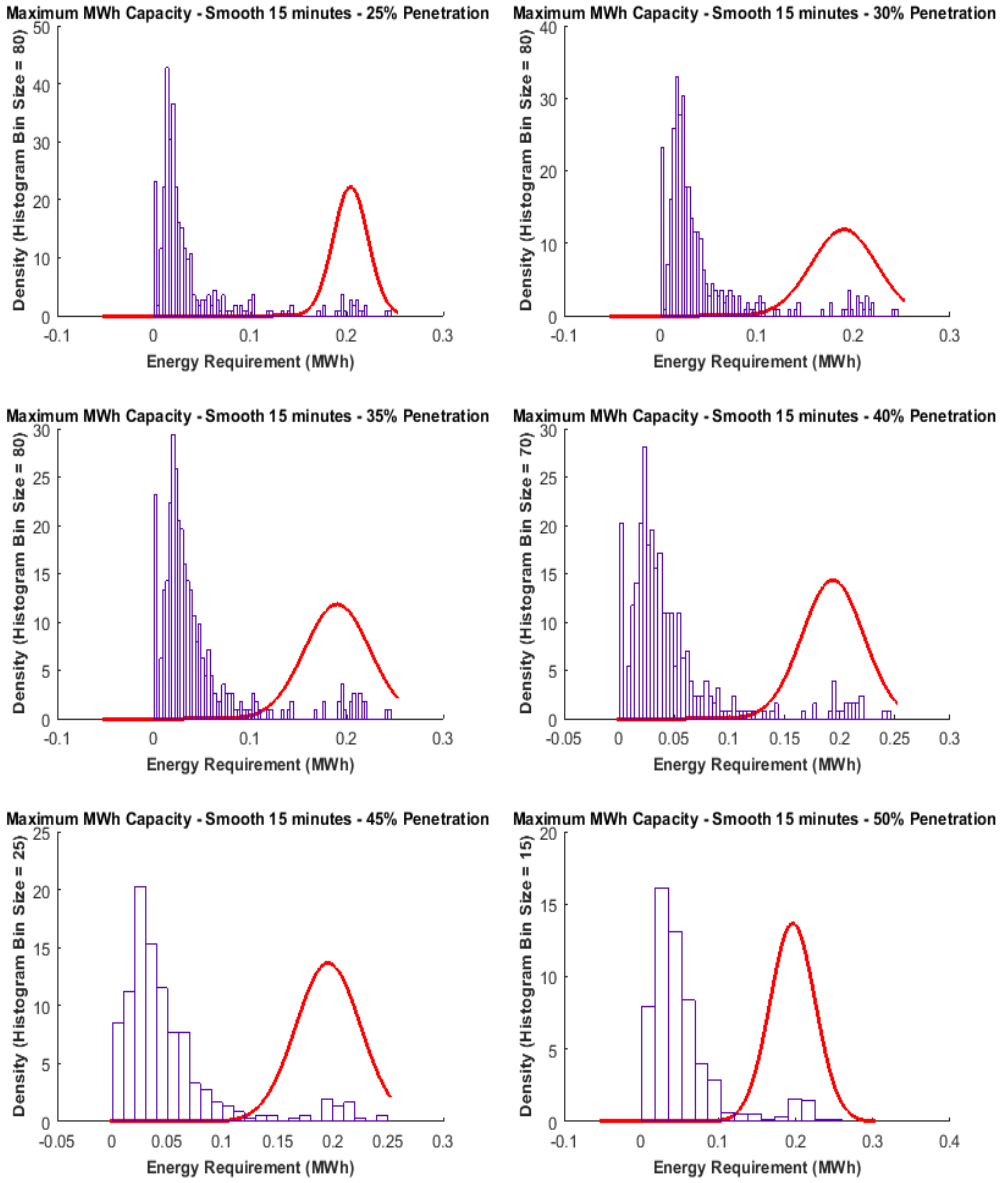

Figure C.3: Fitted Distribution 15 minute smoothing 25%-50% MWh Capacity.

Figure C.4 shows the plots for 30 minute smoothing for 10%-35% PV penetration MW Capacity.

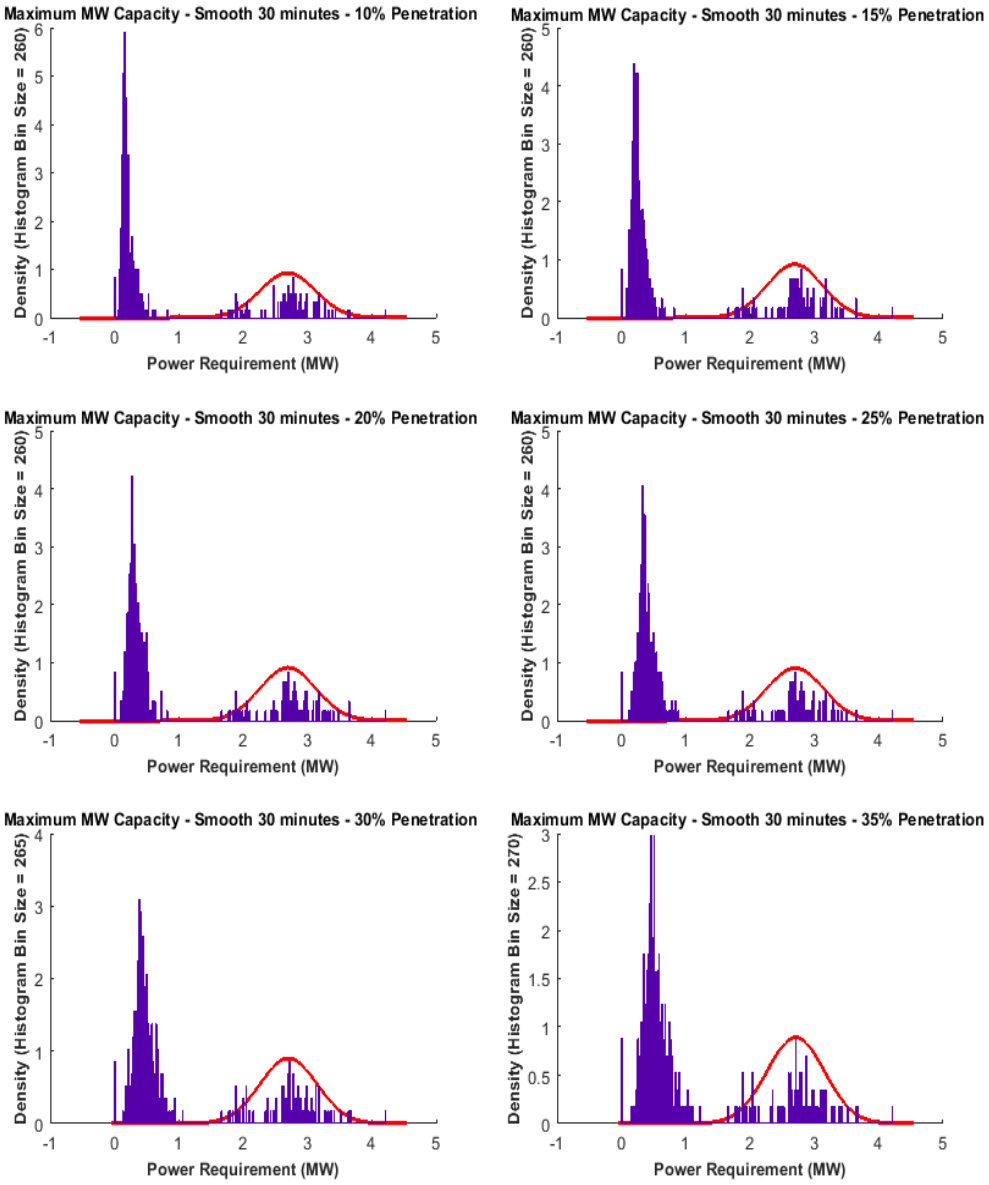

Figure C.4: Fitted Distribution 30 minute smoothing 10%-35% MW Capacity.

Figure C.5 shows the plots for 30 minute smoothing for: 40%-50% PV penetration MW Capacity, and 10%-20% PV Penetration MWh capacity.

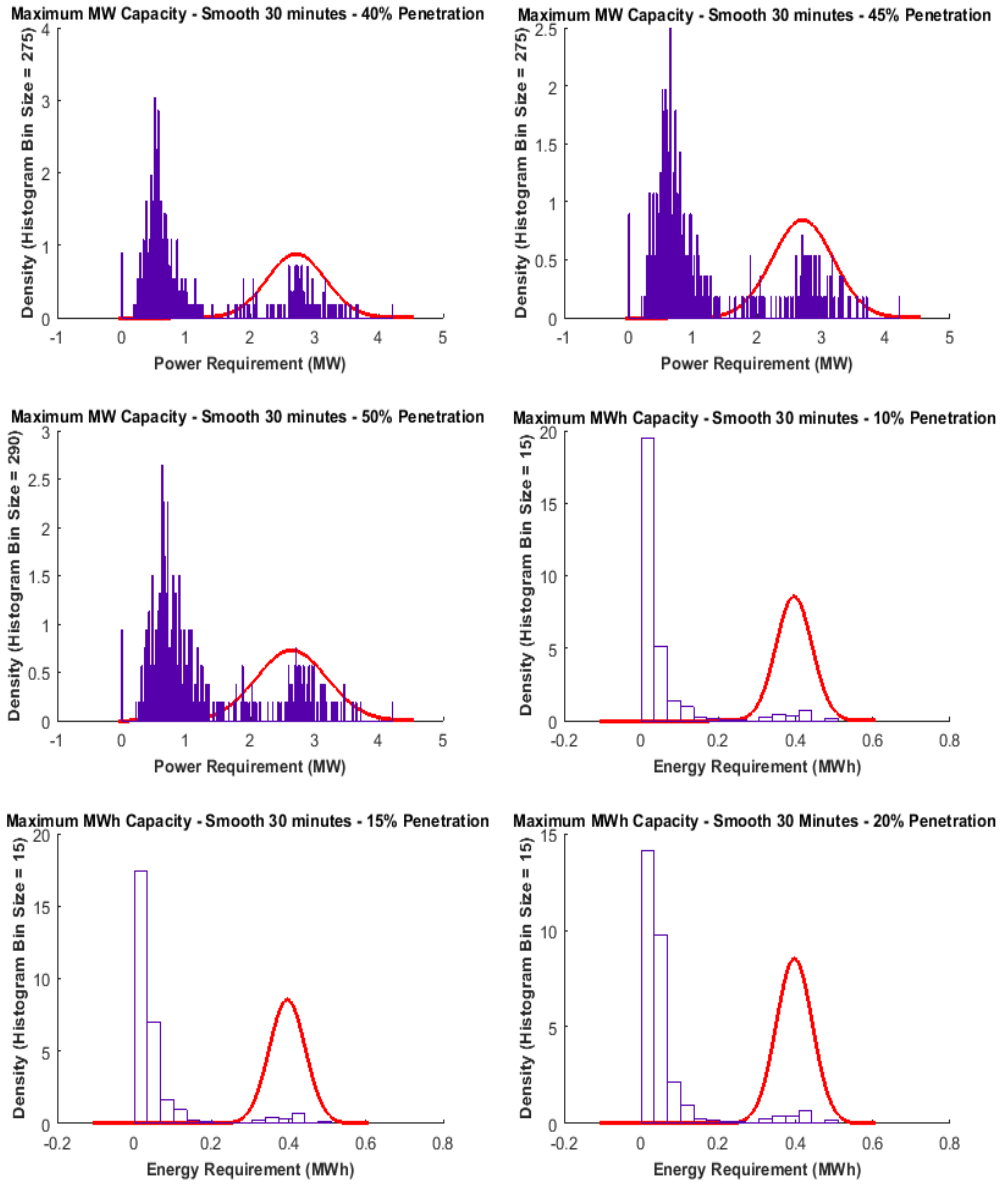

Figure C.5: Fitted Distribution 30 minute smoothing: 40%-50% MW Capacity and 10%-20% MWh Capacity.

Figure C.6 shows the plots for 30 minute smoothing for 25%-50% PV Penetration MWh capacity.

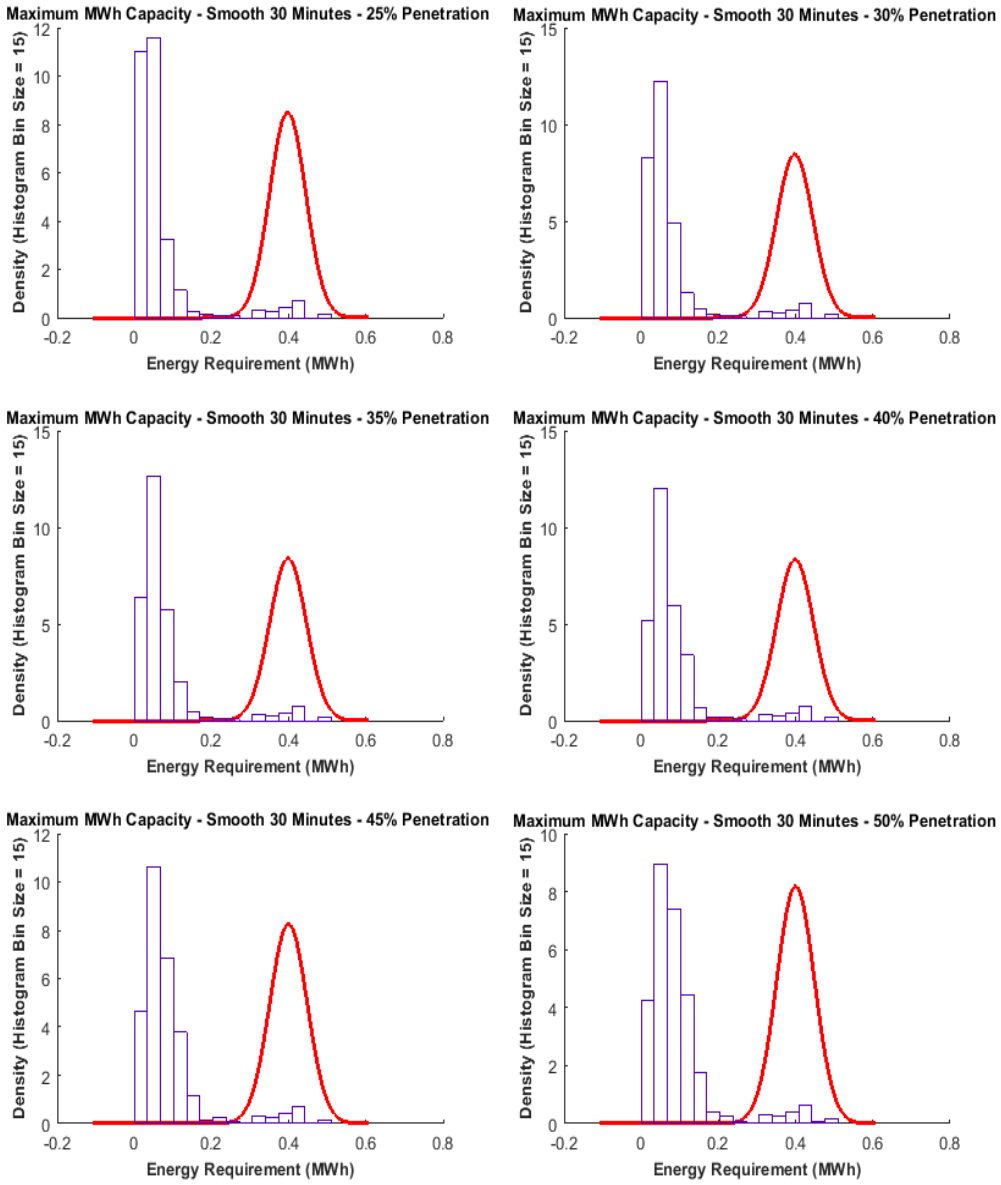

Figure C.6: Fitted Distribution 30 minute smoothing 25%-50% PV Penetration MWh Capacity.

Figure C.7 shows the plots for 60 minute smoothing for 10%-35% PV penetration MW Capacity.

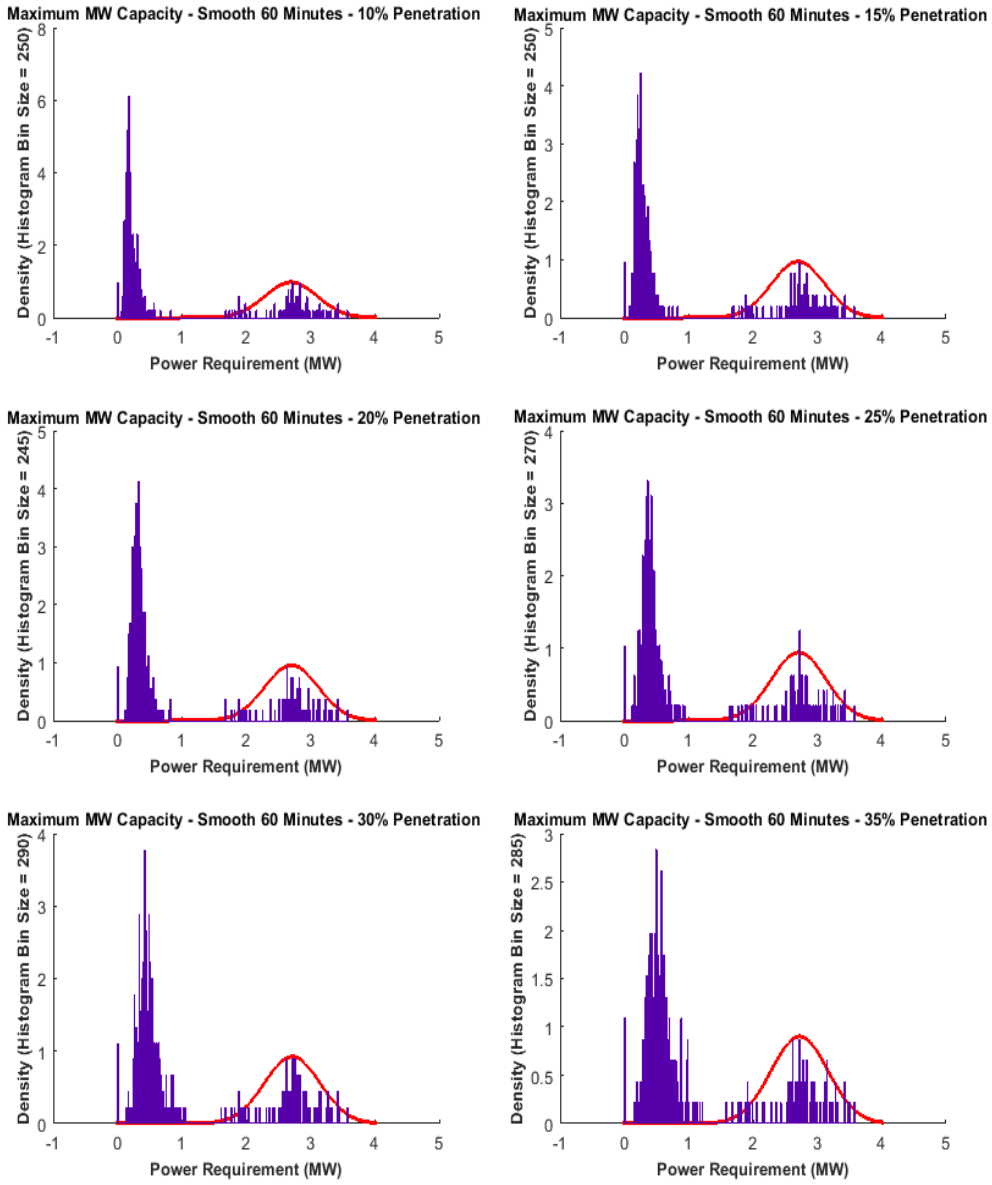

Figure C.7: Fitted Distribution 60 minute smoothing 10%-35% MW Capacity.

Figure C.8 shows the plots for 60 minute smoothing for 40%-50% PV penetration MW Capacity, and 10%-20% PV Penetration MWh capacity.

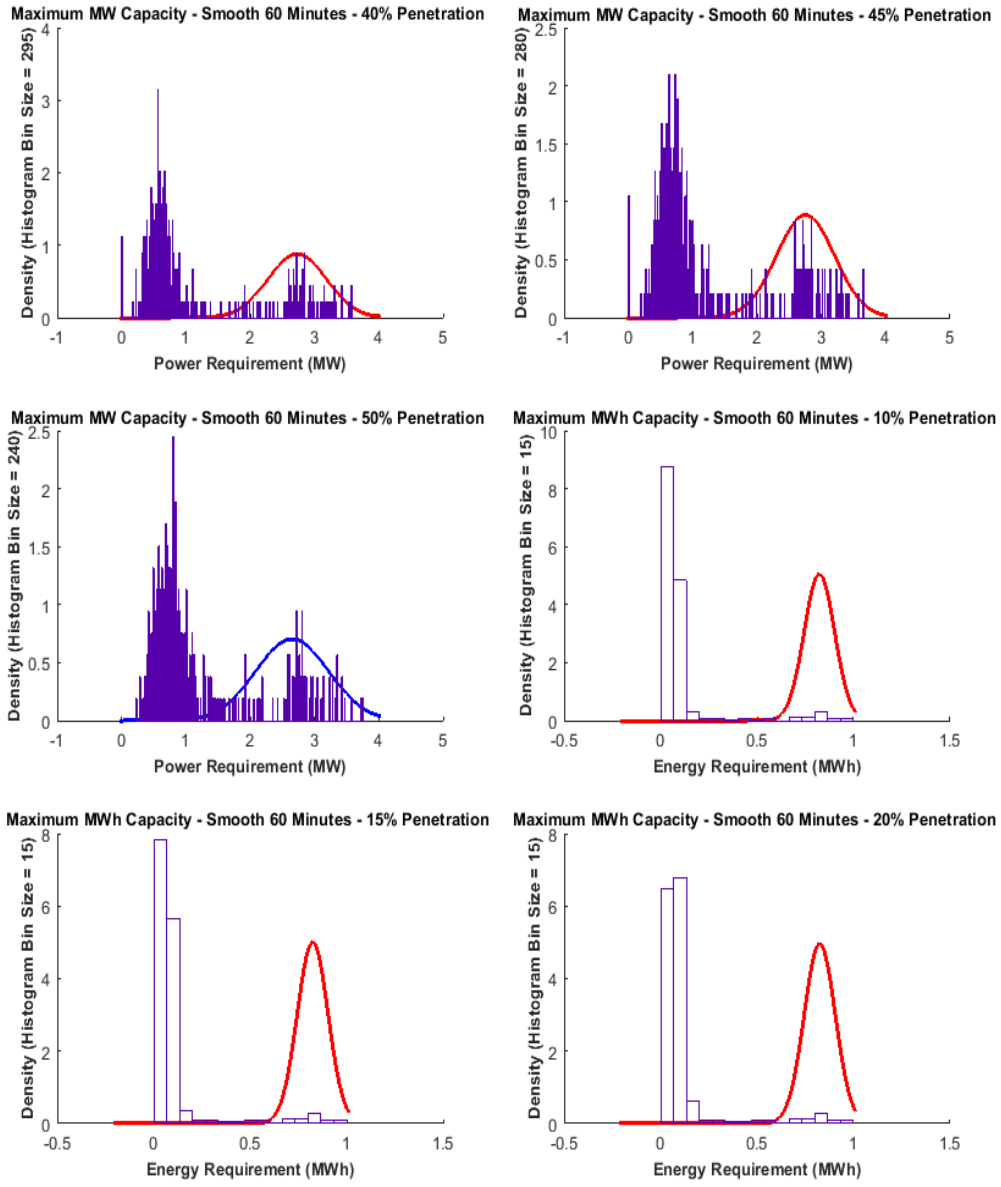

Figure C.8: Fitted Distribution 60 minute smoothing 40%-50% MW Capacity and 10%-20% PV Penetration MWh capacity.

Figure C.9 shows the plots for 60 minute smoothing for 25%-50% PV penetration for MWh Capacity.

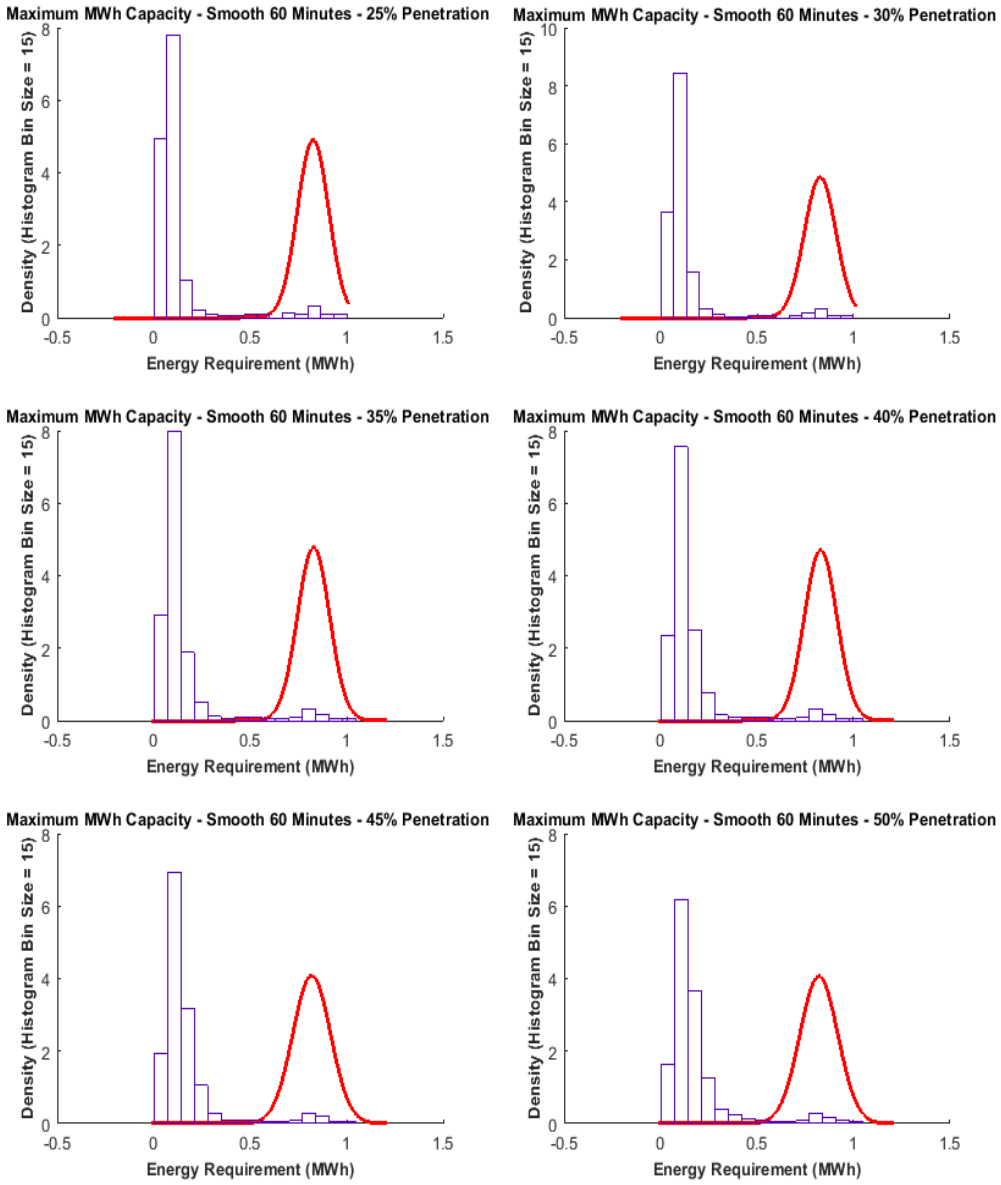

Figure C.9: Fitted Distribution 60 minute smoothing 25%-50% MWh Capacity.

Figure C.10 shows the plots for 90 minute smoothing for 10%-35% PV penetration MW Capacity.

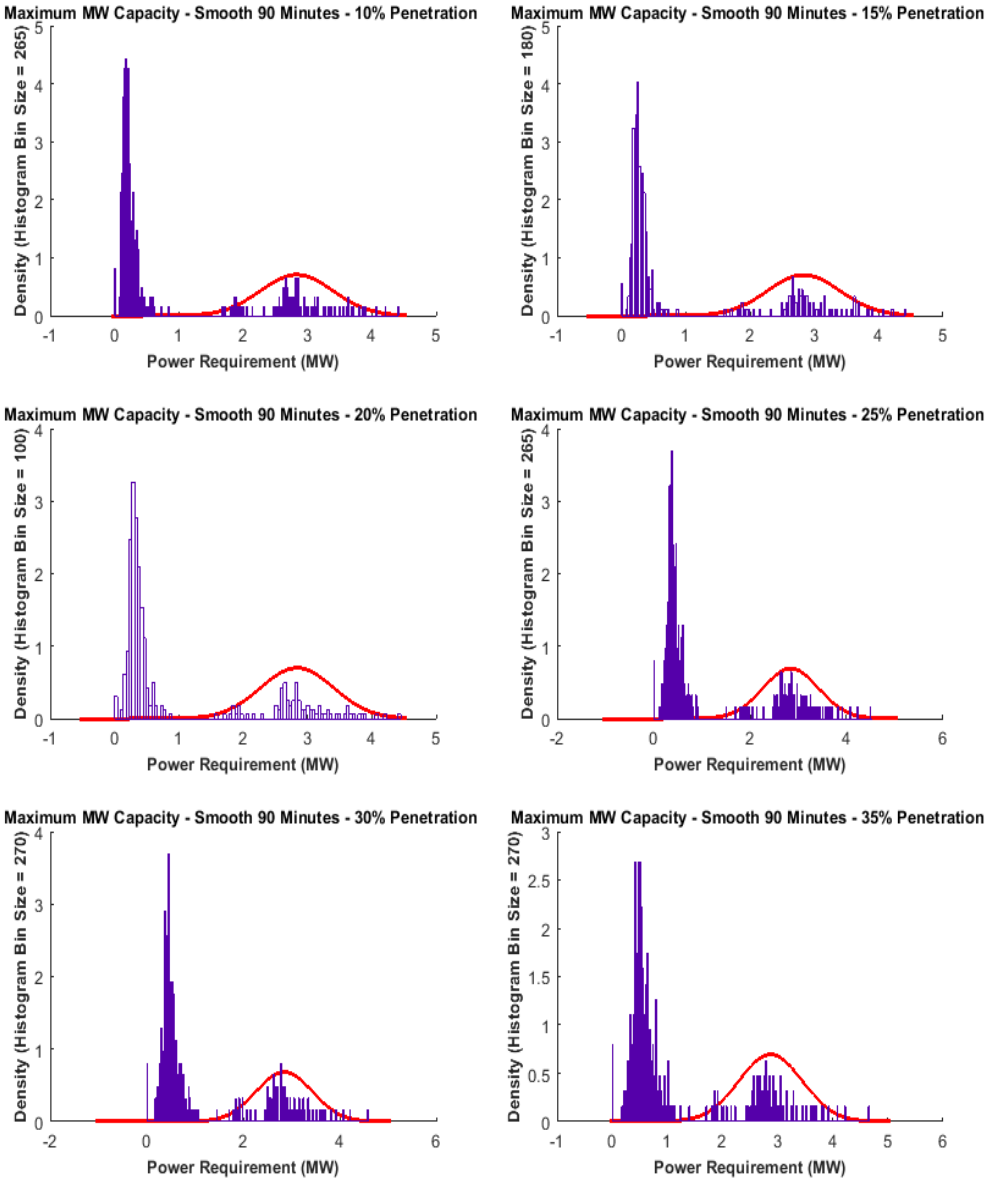

Figure C.10: Fitted Distribution 90 minute smoothing 10%-35% MW Capacity.

Figure C.11 shows the plots for 90 minute smoothing for 40%-50% PV penetration for MW Capacity, and 10%-20% PV Penetration MWh capacity.

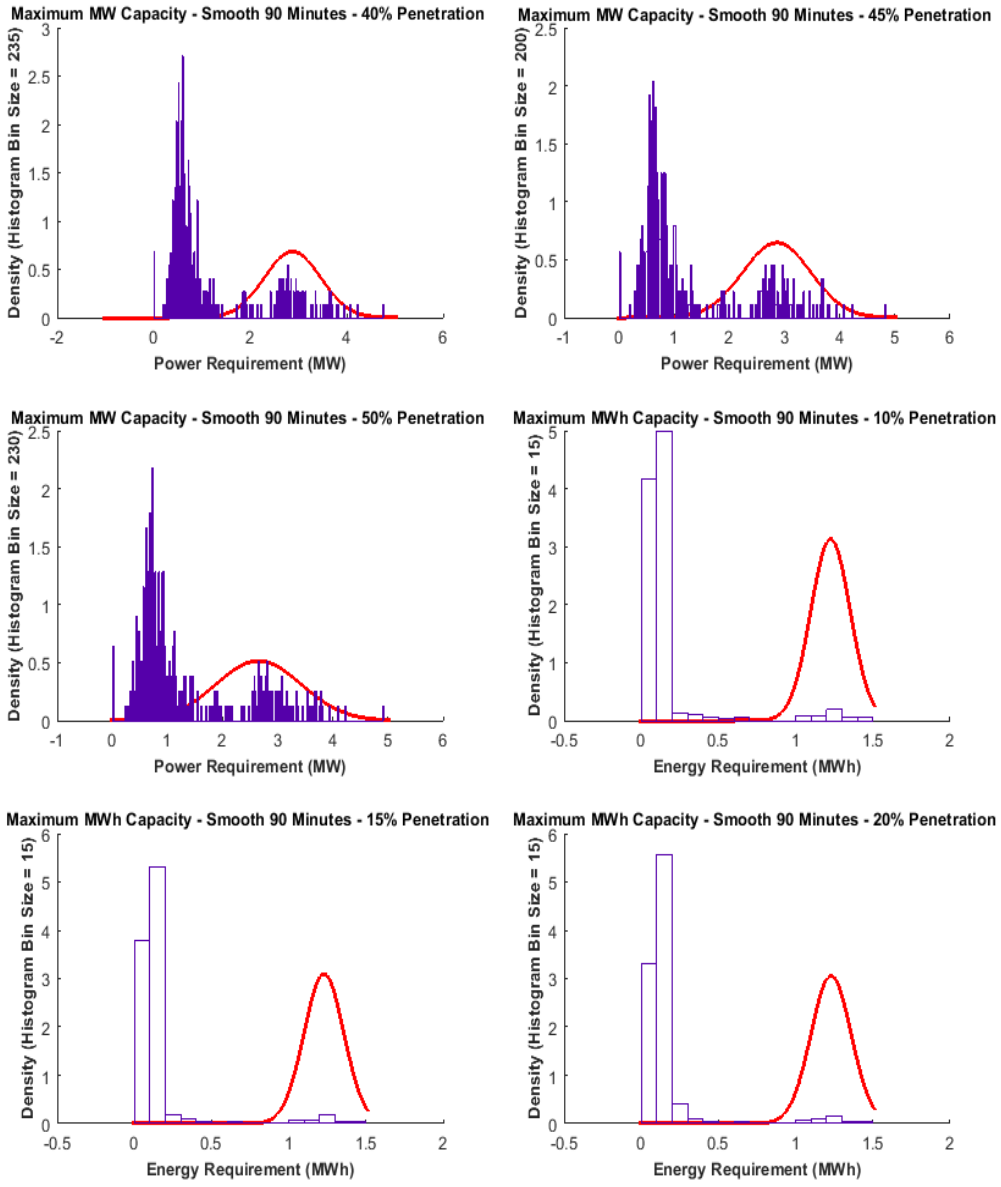

Figure C.11: Fitted Distribution 90 minute smoothing 40%-50% PV penetration MW Capacity and 10%-20% PV penetration MWh Capacity.

Figure C.12 shows the plots for 90 minute smoothing for 25%-50% PV penetration MWh Capacity.

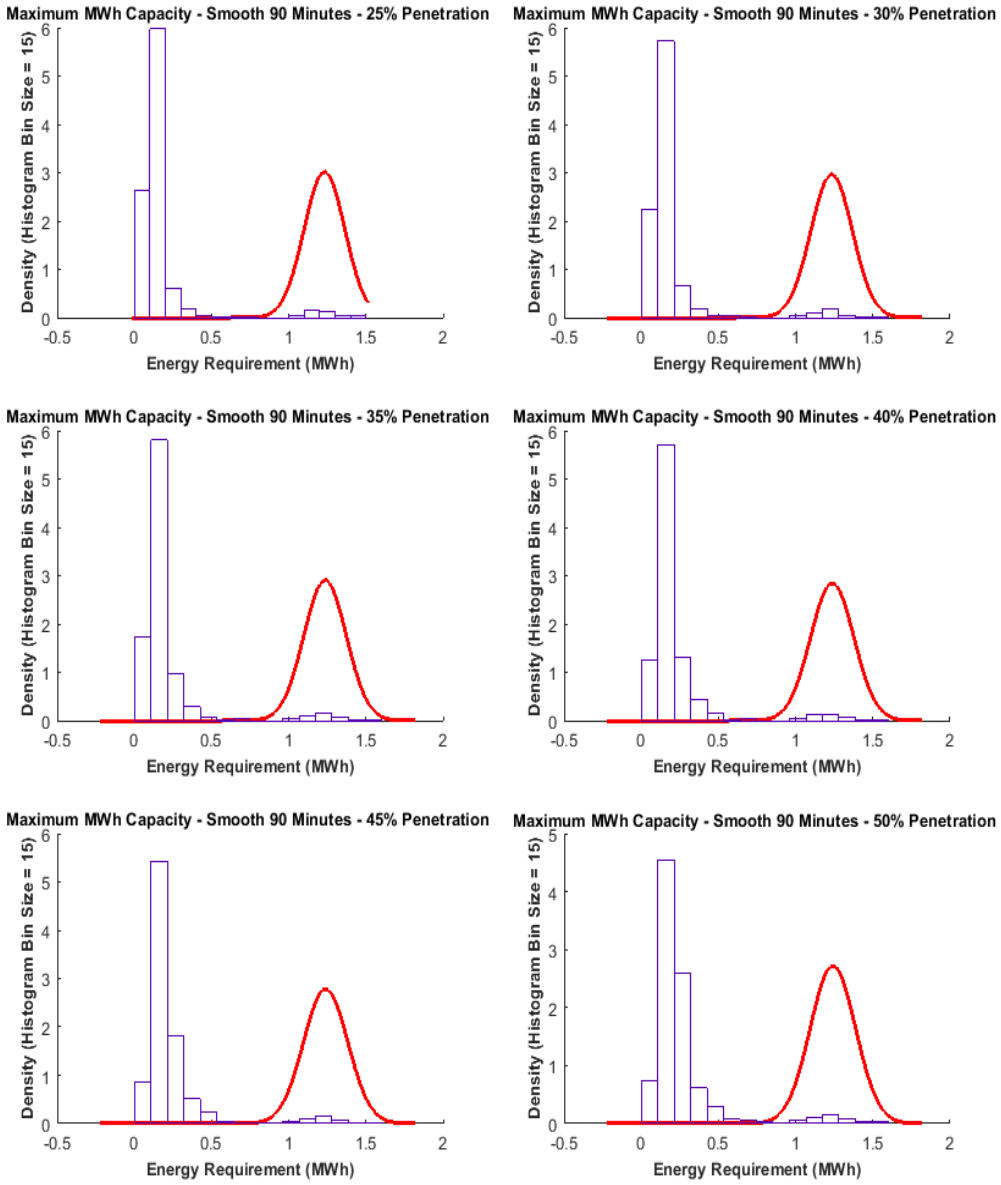

Figure C.12: Fitted Distribution 90 minute smoothing 25%-50% PV penetration MWh Capacity.